Available online at www.sciencedirect.com
SCIENCE DIRECT
Precambrian Research 147 (2006) 124–147
Precambrian Research
www.elsevier.com/locate/precamres

Geochemistry and sedimentary petrology of Archean clastic sedimentary rocks at Mt. Goldsworthy, Pilbara Craton, Western Australia: Evidence for the early evolution of continental crust and hydrothermal alteration

Kenichiro Sugitani [a,*], Fumiaki Yamashita [b], Tsutomu Nagaoka [c], Koshi Yamamoto [d], Masayo Minami [e], Koichi Mimura [d], Kazuhiro Suzuki [e]

[a] *Department of Environmental Engineering and Architecture, Graduate School of Environmental Studies, Nagoya University, Nagoya 464-8601, Japan*
[b] *Department of Earth and Planetary Sciences, Graduate School of Science, Nagoya University, Nagoya 464-8602, Japan*
[c] *School of Informatics and Sciences, Nagoya, University, Nagoya 464-8601, Japan*
[d] *Department of Earth and Environmental Sciences, Graduate School of Environmental Studies, Nagoya University, Nagoya 464-8601, Japan*
[e] *Nagoya University Center for Chronological Research, Nagoya 464-8602, Japan*

Received 2 November 2005; received in revised form 14 February 2006; accepted 19 February 2006

Abstract

Geochemical and petrological analyses of Archean clastic metasedimentary rocks at Mt. Goldsworthy in the Pilbara Craton, Western Australia reveal the early evolution of continental crust and the Earth's surface environment. The succession correlative to the ca. 3.4 Ga Strelley Pool Chert is composed dominantly of silicified medium-grained to very coarse-grained sandstone, siltstone and shale, with minor chert and precipitative beds of nahcolite and barite. The sandstone is generally rich in detrital quartz, with the coarse-grained sandstone containing abundant, very well rounded mono-crystalline quartz that is assumed to be derived from older sedimentary rocks. The recycled detritus is mixed with first-cycle detrital material such as feldspar and barite that is sourced from reworked precipitative beds. The sandstone also contains zircon, Fe–Ti oxides, sulfides and lithic fragments of various origins including mafic-ultramafic volcanic rocks, sedimentary and possibly metamorphic rocks.

Al–Ti–Zr systematics indicates that the source area for the Mt. Goldsworthy clastic metasedimentary rocks was locally subjected to hydrothermal alteration. Reaction with the acid solution resulted in Al-dissolution and the formation of Zr- and Ti-enriched residual detrital material. The enrichment in heavy rare earth elements and low Al_2O_3/TiO_2 values of Mt. Goldsworthy samples reflects the inflow of the residual zircon- and Ti-oxides-enriched detritus. Th/Sc, La/Sc and Eu/Eu* ratios that are unaffected by contamination by the residual detritus indicate a mixed provenance with a significant contribution from granitoid rocks. The presence of detrital zircon older than 3.5 Ga was also demonstrated in this study.

Keywords: Pilbara; Archean; Mt. Goldsworthy; Hydrothermal alteration; Crustal evolution; Trace element geochemistry

1. Introduction

The nature of crustal evolution during the early Precambrian is a major issue in the earth sciences. For example, Taylor and McLennan (1985) examined

* Corresponding author. Tel.: +81 52 789 4865; fax: +81 52 789 4770.
E-mail address: sugi@info.human.nagoya-u.ac.jp (K. Sugitani).

0301-9268/$ – see front matter © 2006 Elsevier B.V. All rights reserved.
doi:10.1016/j.precamres.2006.02.006

compositional change within Precambrian shales and proposed that the upper crust underwent significant compositional change at the Archean–Proterozoic boundary. In contrast, Condie (1993) describes the early evolution of granite in the upper crust, subsequently supported by Eu/Eu* data from Precambrian shales (Gao and Wedepohl, 1995). The chemical and mineralogical composition of clastic sedimentary rocks is controlled by various factors such as source rock composition, weathering and sedimentation processes such as mechanical sorting, decomposition and diagenesis. Sedimentary rocks also provide valuable evidence of crustal evolution during early Precambrian time, where the source rock has been destroyed by erosion (e.g., Bhatia and Crook, 1986; Condie and Wronkiewicz, 1990; Cullers et al., 1988; Fedo et al., 1996, 1997; Feng and Kerrich, 1990; Hofmann, 2005; Hofmann et al., 2003; Holland, 1984; Johnsson, 1993; McLennan et al., 1983; Naqvi et al., 2002; Nesbitt et al., 1996; Sugitani et al., 1996; Taylor and McLennan, 1985; Wronkiewicz and Condie, 1987, 1989). The early (>3.0 Ga) evolution of continental crust within the Pilbara Craton, Western Australia, has been investigated using the record of erosion of ~3.5 Ga granitoid basement (Buick et al., 1995), U–Pb zircon ages (McNaughton et al., 1993; Smithies et al., 1999; Thorpe et al., 1992).

In this study, we describe the geochemistry and mineralogy of Archean metasedimentary rocks (shale, arenite and wacke) at the southwest margin of Mt. Goldsworthy in the northeastern Pilbara Craton, Australia. The Mt. Goldsworthy metasedimentary succession was first described in detail by Sugitani et al. (2003), who suggested source rocks of greenstones, volcaniclastic rocks and reworked precipitative beds (nahcolite and barite) within a continental margin setting. The metasedimentary rocks are quartz-rich, yet a granitoid provenance has not been adequately considered. Given the scarcity of clastic sedimentary rocks older than 3.3 Ga in the Pilbara Craton, the Mt. Goldsworthy metasedimentary succession contains important information about crustal evolution and related surface processes during the earth's early history. We discuss sedimentary provenance, alteration of source rocks and factors controlling trace element geochemistry in the context of Archean crustal evolution and surface environment.

2. Geological background

2.1. General geology

The Pilbara Supergroup of the eastern Pilbara Craton comprises, in ascending stratigraphic order, the Warrawoona, Kelly, Sulphur Springs and Gorge Creek Groups (Van Kranendonk et al., 2004). The sedimentary succession at Mt. Goldsworthy is located 100 km east of Port Hedland (Fig. 1), and was previously assigned to the Corboy Formation of the Gorge Creek Group (Smithies, 2002; Sugitani et al., 2003). The most recent lithostratigraphic scheme for the Pilbara Craton places the lower part of the Goldsworthy succession within the Kelly Group (Van Kranendonk et al., 2004), and is correlated with the ca. 3.4 Ga Strelly Pool Chert based on lithology and stratigraphy (Van Kranendonk, pers. commun.). The type locality for the Strelley Pool Chert, within the East Strelley greenstone belt, consists of basal quartz-rich sandstone with minor conglomerate, silicified laminated carbonates, mafic volcaniclastic rocks and local pseudomorphic evaporitic minerals (Lowe, 1980, 1983).

The Mt. Goldsworthy metasedimentary succession (the Strelley Pool Chert) overlies heavily altered mafic to ultramafic, volcanic and volcaniclastic rocks of the

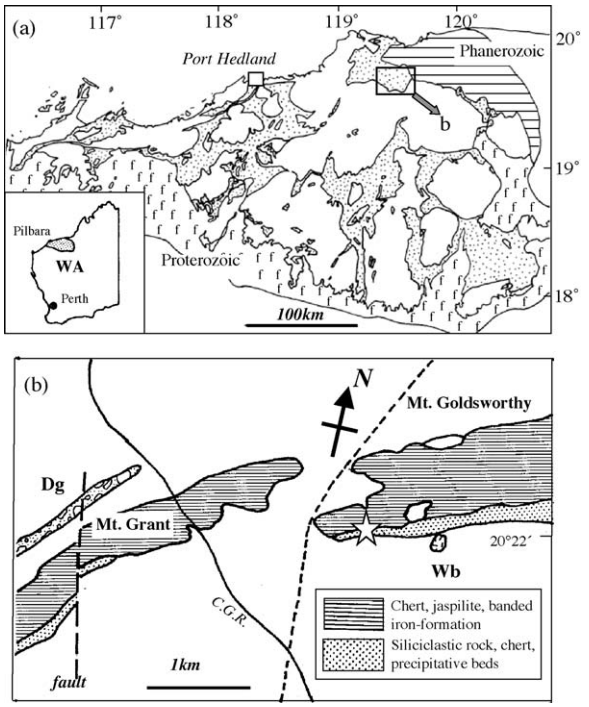

Fig. 1. (a) Simplified geological map of the Pilbara area. The stippled area shows greenstone belt. (b) Geological map of the Mt. Goldsworthy area (after Smithies, 2002). C.G.R. is Coongan–Goldsworthy Road. Wb and Dg are basaltic members of the Warrawoona Group and clastic sedimentary rocks of the De Grey Group, respectively. Siliciclastic rock, chert and precipitative bed correlate to the Strelley Pool Chert of the Kelly Group, whereas chert, jaspilite and banded iron-formation correlate possibly to the Nimingarra Iron Formation of the Gorge Creek Group. Thus the sedimentary succession tends to be younger from the southeast to the northwest. The star indicates the sampling location. Blank areas are Quaternary sediments.

Warrawoona Group, though not yet assigned to any specific members (Smithies, 2002; Sugitani et al., 2003). The 3.43–3.52 Ga Warrawoona Group consists of the Coonterunah, Talga Talga, Coongan and Salgash Subgroups (Van Kranendonk et al., 2004). These subgroups consist dominantly of mafic and ultramafic igneous rocks (tholeiitic basalt and gabbro, high-Mg basalt, peridotitic komatiite, high-Al basalt) (Hickman, 1983; Glikson and Hickman, 1981). Green et al. (2000) undertook trace element study of basalts of the Coonterunah and Warrwoona Groups and show that the rocks were contaminated by a ca. 25% felsic crustal material. On the basis of this data, Green et al. proposed that these rocks were erupted onto continental basement, although Barley (1993) concluded that the Warrawoona Group formed within volcanic-arc and near-arc settings. Minor intermediate to felsic volcanic rocks, chert and volcaniclastic rocks of the Warrawoona Group are known as the Panorama and Duffer Formations; the Panorama Fomration is locally overlain by the Strelley Pool Chert (DiMarco and Lowe, 1989b,c).

2.2. Stratigraphy and sedimentary environment

A simplified stratigraphic column for the southwestern margin of the Mt. Goldsworthy succession is shown

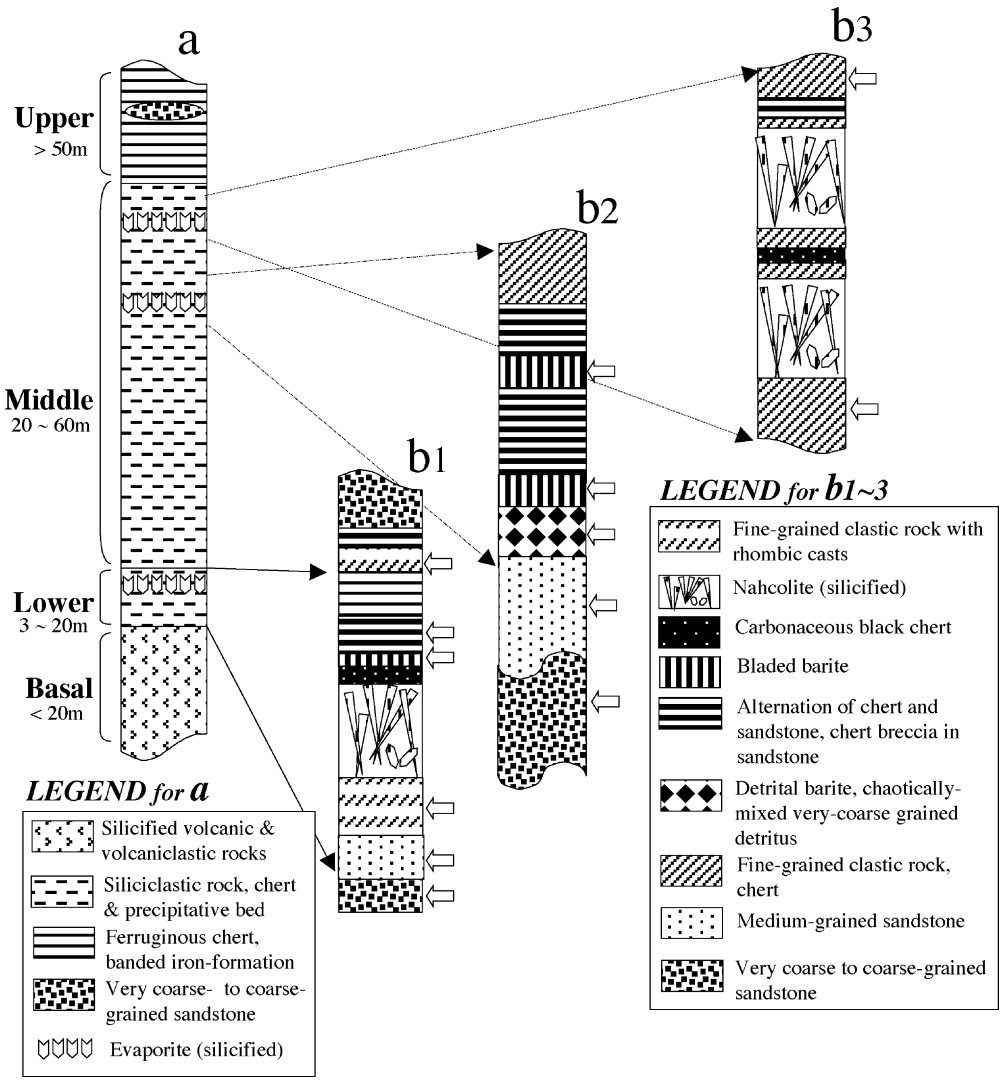

Fig. 2. (a) Representative stratigraphic column of the volcanic–sedimentary succession at Mt. Goldsworthy (modified from Sugitani et al., 2003), with ranges of thicknesses for each unit shown. The basal unit correlates to the Warrawoona Group volcanic and volcaniclastic rocks. (b) Details of the stratigraphic column. Note that the thickness of each lithology is modified to various degrees, in order to show the lithological variation clearly. The white arrows show the horizons sampled for this study.

in Fig. 2. The metasedimentary succession overlies silicified, mafic to ultramafic rocks of the Warrwoona Group, and is divided into lower, middle and upper units (Sugitani et al., 2003). The lower and middle sedimentary units consist of fine-grained to very coarse-grained clastic rocks (shale and sandstone) with minor chert and precipitative beds. The upper sedimentary unit is dominated by laminated to banded ferruginous chert and banded iron-formation with minor lenses and beds of sandstone, which is probably assigned to the Gorge Creek Group (the Nimingarra Iron Formation) (Smithies, 2002).

Two types of silicified precipitative beds are identified. The first is composed of silicified large subvertical crystals up to 40 cm in length that have been interpreted as nahcolite ($NaHCO_3$) (Sugitani et al., 2003). Archean nahcolite has been previously reported from the Barberton greenstone belt (Lowe and Worrell, 1999). Nahcolite is stable under high CO_2 partial pressure and is therefore considered evidence for high levels of atmospheric CO_2 during the Archean. The second type of precipitative bed is composed of closely packed subvertical bladed barite crystals ($BaSO_4$), or detrital grains of barite.

Nahcolite is most likely of evaporitc origin, suggesting that the lower and middle unit had deposited at the shallow to sub-aerial environment, whereas the upper unit deposited sub-aqueously. The Mt. Goldsworthy metasedimentary succession defines an overall upward fining and deepening trend and records sedimentary processes and environment possibly at a continental margin setting (Sugitani et al., 2003).

2.3. Lithology and sedimentary petrology

The Mt. Goldsworthy metasedimentary succession is pervasively silicified and most of the framework grains were replaced by microcrystalline to granular quartz and sericite, with the exception of detrital quartz, mica, zircon, sulfides and Fe–Ti oxides (e.g., oxidized ilmenite and Ti-rich magnetite). The origin of the altered framework grains was identified on the basis of grain shape, mineral composition and internal texture. Detailed descriptions and interpreted origins of silicified framework grains are summarized in Table 1.

2.3.1. Coarse- to very coarse-grained sandstone

Coarse- to very coarse-grained sandstone, including pebbly sandstone, occurs in the lower horizons of the lower and middle units (Fig. 2b). Coarse-grained sandstone lenses and beds are intercalated with ferruginous chert and banded iron-formation in the upper unit (Fig. 2a).

2.3.1.1. Lower unit. Coarse- to very coarse-grained sandstone in the lower unit is rich in matrix and cement composed dominantly of microcrystalline quartz, especially within the pebbly sandstone. Very angular to rounded pebbles and framework grains of lithic

Table 1
Detailed descriptions and assumed origins of silicified lithic fragments and some framework grains

Type	Description	Origins/sources
SCT	Free from terrigenous detritus. Fine particles of oxides, carbonates and carbonaceous matter comprising sedimentary and diagenetic structures such as lamination and spherules	Chemical and biogenic sediments (chert and carbonate)
TCS	Dispersed fine sand-sized detrital quartz, sericite and/or some other probably authigenic and metamorphic minerals such as epidote and apatite	Fine-grained terrigenous clastic sediments (shale)
FLV	Significant amounts of sericite. Lack of detrital quartz. Rarely crescent-shaped	Possibly felsic volcanic rocks
PYG	Very angular shaped with occasional concave outer surfaces and bubbles inside. Abundant fine TiO_2-particles and sericite. Poor development of crystal phantoms and pseudomorphs	Pyroclastics
MFV	Crystal phantoms and skeletons identified by fine TiO_2 particles. Well preserved spinifex or microlite texture	Mafic to ultramafic volcanic rocks
MET	Granular to elongated (with preferred orientation) quartz	Metamorphic rocks
QSM	Sericite-dominant quartz-sericite mosaic. Angular to lath-shaped	Feldspar lath
PCT	Trace amount of unidentified fine impurities (oxidized euhedral pyrite, and/or carbonate particles). No distinct sedimentary structure. Occasional chalcedonic extinction figure and megaquartz inside	Chemical sediments, veins, cement and/or pure precipitates (sedimentary chert, chert veins, carbonate and evaporite): cannot always been descriminated from SCT

Note: This table is modified from Sugitani et al. (2003). Also see the references therein.

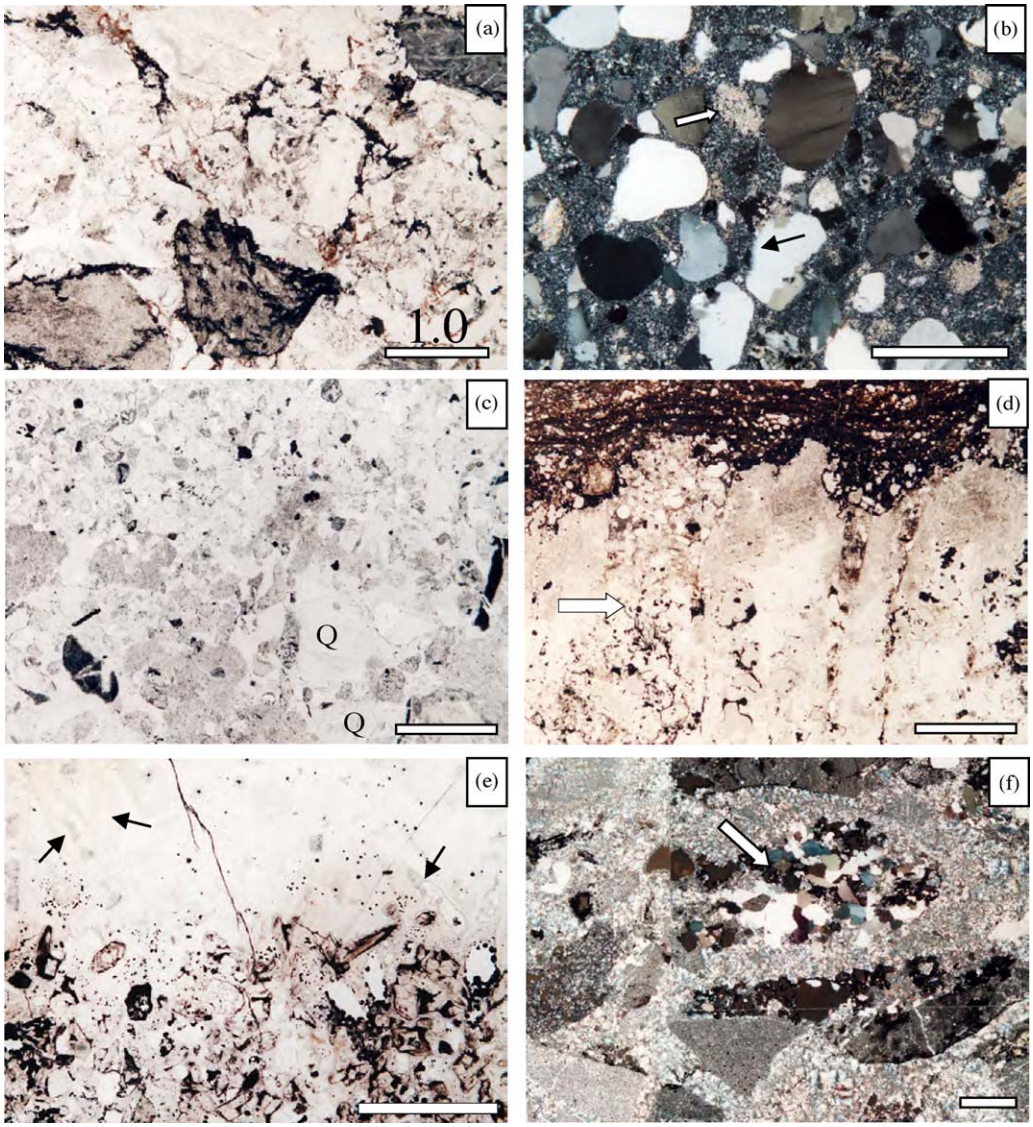

Fig. 3. Photomicrographs of Mt. Goldsworthy clastic rocks and precipitative beds (barite). (a) Very coarse-grained lower unit sandstone. Dark fragments are mafic to ultramafic volcanics. (b) Coarse-grained middle unit sandstone rich in rounded monocrystalline quartz. The white arrow shows a silicified feldspar lath. Note that the outline of some quartz grains appears blurred (e.g. black arrow) due to replacement by microcrystalline quartz. (c) Medium-grained middle unit sandstone. The upper half is enriched in opaque minerals and zircon, while the lower half is enriched in sericite. Note the very coarse-grained quartz grain (Q), nearly 1 mm in length, set within the sericite rich portion of the sample, indicating sediment immaturity. Opaque minerals in the upper portion are dominated by aggregations of fine TiO_2. (d) Subvertical bladed barite crystals (white) overlain by a detrital layer. Note that the barite crystal heads are eroded. The interstices of barite crystals are filled with dominantly quartz detritus (white arrow). (e) Layer composed dominantly of detrital barite (lower half of image) and associated silicified lenticular crystals of unknown origin (arrows). (f) Very coarse-grained sandstone associated with detrital and bladed barite layers in the middle unit. Note sandstone fragments (white arrow). Plane polarized light for (a, c–e). Crossed polarized light for (b and f). Scale bars are 1 mm.

fragments and minor quartz, feldspar and barite are chaotically mixed (Fig. 3a). The pebbles are up to 1 cm in length, though very poorly sorted. Resistant accessory minerals such as muscovite, zircon, sulfides and Fe–Ti oxides are also present. Most lithic clasts are cherts including silicified fragments of precipitative beds: Mafic to ultramafic clasts are also present as a subordinate component.

2.3.1.2. Middle unit. Coarse- to very coarse-grained sandstone in the middle unit is also matrix and cement-rich (>30%) and locally contains mud laminae. The

degree of textural maturity varies from sample to sample and even within a thin section. The middle unit contains the same framework grains and accessory minerals identified in the lower unit, but has a greater proportion of detrital quartz, feldspar and mica. Relatively large and very well rounded monocrystalline quartz is locally abundant, and is spatially associated with feldspar laths and angular to very-angular detrital quartz grains (Fig. 3b). The rims of detrital quartz grains are often replaced by microcrystalline quartz. Secondary growth rims are also observed on detrital quartz grains. Detrital mica occurs as flakes and rarely as composite mosaic grains.

2.3.1.3. Upper unit. Sandstone lenses and beds in the upper unit of ferruginous chert and banded iron-formation are generally quartz-rich and matrix-poor in comparison with middle unit sandstone. Some upper unit sandstones are quartz arenites.

2.3.2. Medium-grained sandstone

Medium-grained sandstone, in particular that in the middle unit, is enriched in feldspar, opaque minerals, mica flakes and locally volcaniclastic fragments, compared with coarse- to very coarse-grained sandstone. Fine-grained, sericite-rich layers indicate original mud laminae within the sandstone beds; sulfide, zircon and Fe–Ti oxides often comprise laminae (Fig. 3c).

2.3.3. Fine-grained clastic rocks

Fine-grained clastic rocks are similar in appearance to chert and are composed dominantly of microcrystalline quartz. The clastic origin of these rocks is evident from the presence of disseminated fine silicate and dispersed detrital quartz grains.

The fine-grained clastic rocks can be divided into two main types depending upon the presence or absence of detrital quartz. Fine-grained clastic rocks deficient in detrital quartz occur within the lower unit and locally at the base of the middle unit as beds less than 1 m in thickness. The rocks locally display cross lamination (Sugitani et al., 2003). This rock type lacks coarse terrigenous detritus and is composed of granular microcrystalline quartz, fine silicate minerals and Ti-oxide. The rock is characterized by rhombic casts, possibly silicified rhombic carbonate (Sugitani et al., 2003; Fig. 6d). The detrital quartz-bearing sediment originated from a siliceous shale or siltstone and is a major component of the upper portion of the middle unit. This rock type contains sericite, Fe-oxides, muscovite flakes and fine TiO_2 grains. Rhombs composed of iron oxides suggest the former presence of iron-bearing carbonate. Laminations are defined in many cases by fine- to medium-grained detrital quartz.

2.3.4. Barite and related lithologies

The Mt. Goldsworthy metasedimentary succession contains silicified barite-bearing beds (Fig. 2b_1 and 2b_2). The beds are composed of sub-vertical bladed barite crystals and detrital barite grains (Fig. 3d and e). The barite beds are generally associated with layers of abundant very coarse-grained, angular, lithic fragments mixed chaotically with quartz sand, detrital barite grains and trace amount of spherules of possible impact or volcanic origin up to 500 μm in diameter. The framework grains are cemented by microcrystalline quartz showing a chalcedonic extinction figure (Simonson, 1985). These features are basically similar to the very coarse-grained sandstone in the lower sedimentary unit. However, the barite lithology contains earlier silicified sandstone fragments (Fig. 3f).

3. Samples and analytical methods

Fifty-six samples of clastic sedimentary rocks were chosen for geochemical analysis (Fig. 2): 12 samples of very coarse- to coarse-grained sandstone, including 1 from the lower unit, 9 from the middle unit and 2 from the upper unit; 15 samples of medium-grained sandstone, including 6 from the lower unit and 9 from the middle unit; 15 samples of fine-grained clastic rocks, including 6 from the lower unit and 9 from the middle unit; 14 samples of barite and associated lithologies, including 3 from the lower unit and 11 from the middle unit.

Major elements were analyzed by automatic X-ray fluorescence spectrometer (XRF) using fusion glasses made from a 1:5 mixture of powdered sample and $Li_2B_4O_7$ flux (Sugisaki et al., 1977), while Na and K concentrations were analyzed by instrumental neutron activation analysis (INAA). $Carbon_{total}$, H_{total} and S_{total} were determined using an elemental analyzer. Concentrations of minor elements including rare-earth elements (REEs) were determined by XRF, graphite-furnace atomic adsorption spectrometer (GFAA) and inductively coupled plasma mass spectrometer (ICP-MS) and INAA.

Pressed discs made from a 2:3 mixture of powdered sample and binder were analyzed by XRF for Rb, Sr, Zr and Ba (Sugitani and Mimura, 1998). Chromium, Co, Sc, Th, Hf, Ta, Rb and some REEs (La, Ce, Sm, Tb, Yb and Lu) were analyzed by INAA following the method of Shibata et al. (2001). Chromium in some samples not subjected to INAA analysis was determined using GFAA following the method of Sugitani et al. (2002). The REEs

Table 2
Major and trace element concentrations for Mt. Goldsworthy siliciclastic sedimentary rocks

	Very coarse to coarse-grained sandstones											
	Lower unit	Middle unit									Upper unit	
Analysis no.	GW98-1-14	GW95-1-3	GW95-1-4	GW95-1-5	GW95-1-6	GW95-1-7	GW93-1-1	GW93-1-2	GW99-2-6	GW99-2-7	GW95-1-21	GW95-1-29
SiO_2 (wt.%)	97.7	89.81	92.82	96.25	92.87	93.57	>95%	>95%	94.72	93.19	89.37	91.04
TiO_2	0.173	0.161	0.202	0.103	0.256	0.171	0.201	0.236	0.134	0.113	0.11	0.097
Al_2O_3	1.23	2.22	2.80	1.11	2.07	1.99	2.03	2.02	1.97	1.82	0.93	0.76
Fe_2O_3 (total)	0.73	2.25	1.26	0.78	2.19	1.49	0.59	0.37	0.80	1.00	7.00	6.64
MnO	0.040	<0.005	<0.005	<0.005	0.012	0.004	0.004	0.004	0.003	0.060	0.336	0.014
MgO	0.15	<0.05	<0.05	<0.05	0.08	0.04	0.04	0.04	0.02	0.06	0.06	<0.05
CaO	0.06	0.01	0.01	0.02	0.04	0.01	0.04	0.03	0.03	0.21	0.02	0.04
Na_2O	0.03	0.05	0.05	0.04	0.06	0.08	0.07	0.07	0.03	0.04	0.02	0.01
K_2O	0.35	0.65	0.75	0.29	0.53	0.48	0.46	n.d.	0.46	0.41	0.11	0.08
P_2O_5	0.008	0.005	0.006	0.114	0.008	0.004	0.010	0.007	0.007	0.012	0.009	0.008
H_2O (total)	0.29	0.67	0.67	0.32	0.50	0.47	0.41	0.32	0.59	0.50	0.81	0.76
Sc (ppm)	2.49	2.60	3.39	1.53	3.81	1.91	1.85	1.81	3.16	3.02	2.31	1.61
Cr	54.7	53.7	39.8	27.0	76.0	48.5	35.4	44.3	33.4	68.9	22.1	22.8
Co	1.3	*0.7*	*0.4*	<0.5	0.8	<0.5	*0.3*	<0.5	0.7	<0.5	1.6	1
Rb	8	17	23	8	16	15	16	14	13	19	2	
Sr	10	6	4		10	2	4	3	3	8		n.d.
Y	2.69											
Zr	34	43	40	27	84	47	52	69	46	49	38	33
Ba	241	373	318	108	317	145	123	184	166	243	154	79
Hf	0.74	1.03	0.99	0.71	1.80	1.02	1.23	1.73	1.01	1.17	0.91	0.85
Ta		*0.31*				*0.36*	0.36	*0.35*			*0.20*	*0.15*
Th	0.66	3.29	1.74	0.91	2.28	2.15	1.45	2.25	1.62	2.23	0.77	0.89
U		*0.61*	*0.52*	*0.37*	*0.62*	*0.49*		0.71				*0.43*
La (ppm)	2.56	4.21	4.21	2.00	4.71	3.47	3.76	4.58	3.23	3.54	2.81	1.55
Ce	3.92	5.33	6.29	3.12	7.40	5.30	5.83	6.86	5.71	4.69	5.28	2.44
Pr	0.46											
Nd	1.76											
Sm	0.35	0.71	0.72	0.30	0.63	0.51	0.49	0.56	0.43	0.49	0.32	0.26
Eu	0.11	*0.21*	*0.22*				*0.10*	*0.10*			*0.08*	*0.07*
Gd	0.39											
Tb	0.06											
Dy	0.44											
Ho	0.10											
Er	0.31											
Tm	0.05											
Yb	0.34	0.52	0.46	0.22	0.56	0.36	0.38	0.45	0.38	0.37	0.41	0.39
Lu	0.05	0.09	0.08	0.04	0.11	0.07	0.07	0.08	0.07	0.07	0.08	0.07

Table 2 (*Continued*)

	Medium-grained sandstone														
	Lower unit						Middle unit								
Analysis no.	GW99-5-4-2	GW99-5-4-1	GW99-5-2	GW99-5-3	GW98-1-16	GW98-1-17	GW99-2-9	GW99-2-10	GW99-2-12	GW99-2-14	GW99-1-23	GW95-1-8	GW95-1-9	GW95-1-10	GW93-1-4
SiO_2 (wt.%)	94.44	94.29	92.79	88.89	93.80	92.81	91.16	88.91		92.67		90.64	90.15	90.85	94.09
TiO_2	0.347	0.345	0.233	0.594	0.259	0.285	0.393	0.398	0.429	0.307	0.227	0.436	0.502	0.521	0.514
Al_2O_3	1.68	1.64	1.78	2.40	2.70	2.69	3.89	4.75	4.76	3.76	2.30	4.27	4.44	4.25	3.15
Fe_2O_3 (total)	0.62	0.67	1.90	3.64	1.46	1.69	0.28	2.03	0.31	0.23	1.22	0.55	0.60	0.33	1.21
MnO	0.044	0.051	0.012	0.067	0.002	<0.005	0.011	0.006	0.006	0.053	<0.005	0.004	0.004	0.004	0.004
MgO	0.02	0.01	0.02	0.04	0.05	0.04	0.04	0.04	0.07	0.05	0.02	0.07	0.06	0.06	0.05
CaO	0.03	0.02	0.05	0.03	0.06	0.07	0.08	0.02	0.02	0.02	0.02	0.02	0.02	0.14	0.13
Na_2O	0.05	0.04	0.05	0.06	0.05	0.05	0.05	0.07	0.07	0.06	0.07	0.10	0.13	0.13	0.08
K_2O	0.42	0.39	0.43	0.60	0.78	0.76	0.93	1.27	1.16	0.89	0.46	0.99	0.97	0.79	0.61
P_2O_5	0.008	0.007	0.012	0.016	0.011	0.011	0.015	0.012	0.009	0.008	0.006	0.005	0.010	0.017	0.010
H_2O (total)	0.34	0.48	0.59	1.02	0.49	0.50	0.07	0.97	0.83	0.94	0.44	0.95	0.82	0.97	0.90
Sc (ppm)	3.83	3.82	4.09	7.40	5.74	6.31	4.34	5.38	5.13	4.59	3.69	4.84	5.70	5.57	5.50
Cr	38.0	43.0	71.0	79.0	84.0	121.0	81.3	60.2	98.6	64.0	125.0	82.9	108.4	73.0	113
Co	1.5	1.9	0.6	2.0	0.9	*0.6*	*0.8*	0.7	*0.6*	1.0	<0.5	*0.6*	<0.5	0.8	<0.5
Rb	14	13	15	20	21	21	34	39	46	31	17	35	33	24	20
Sr	1	2	6	6	9	19	16	7	11	5	3	6	17	42	20
Y	6.07	5.37	3.92	9.47	4.41	5.33	5.88	6.60	6.62	4.20		5.11	9.29	9.79	8.55
Zr	121	119	80	241	101	126	64	87	99	58	49	69	155	110	130
Ba	179	197	276	300	212	483	244	219	289	220	*91*	180	270	623	471
Hf	2.89	2.66	1.94	5.43	2.21	2.73	1.68	2.11	2.54	1.35	1.21	1.43	3.79	2.76	3.15
Ta	*0.26*	*0.34*		*0.63*			*0.46*	*0.32*	*0.44*	*0.25*		*0.36*	*0.58*	*0.49*	*0.51*
Th	2.15	2.19	1.90	2.92	2.54	3.36	2.29	2.36	2.88	1.64	0.98	2.35	4.29	3.40	4.04
U	*0.96*	*0.94*	*0.80*	*1.28*			*0.63*				*0.59*	*0.70*	*1.15*		*1.30*
La (ppm)	6.17	5.90	5.46	6.48	3.56	4.33	8.10	8.79	7.15	10.05	4.95	5.63	10.65	14.30	8.71
Ce	9.38	10.11	8.62	10.60	5.27	7.55	11.90	11.64	12.49	12.91	7.66	9.66	15.14	20.03	12.86
Pr	1.14	1.09	1.08	1.28	0.65	0.80	1.43	1.39	1.43	1.40		1.05	1.72	2.20	1.66
Nd	3.84	3.66	3.98	4.46	2.44	3.00	5.24	4.76	5.36	4.56		3.97	6.18	7.80	6.19
Sm	0.62	0.59	0.76	0.82	0.52	0.62	0.96	0.85	1.00	0.72	0.62	0.76	1.20	1.35	1.18
Eu	0.19	0.19	0.26	0.27	0.16	0.19	0.24	0.21	0.25	0.17	*0.19*	0.20	0.31	0.32	0.29
Gd	0.66	0.62	0.76	0.97	0.58	0.69	0.90	0.83	0.97	0.58		0.73	1.30	1.30	1.20
Tb	0.12	0.11	0.11	0.18	0.10	0.12	0.15	0.15	0.17	0.10		0.13	0.23	0.22	0.20
Dy	0.91	0.82	0.68	1.39	0.71	0.87	0.97	1.08	1.12	0.68		0.86	1.53	1.54	1.38
Ho	0.21	0.19	0.14	0.33	0.16	0.20	0.22	0.24	0.25	0.16		0.19	0.33	0.34	0.30
Er	0.72	0.65	0.45	1.11	0.53	0.65	0.68	0.77	0.79	0.50		0.62	1.03	1.08	0.95
Tm	0.12	0.11	0.07	0.18	0.09	0.11	0.11	0.12	0.13	0.08		0.10	0.16	0.17	0.15
Yb	0.84	0.78	0.50	1.33	0.63	0.75	0.73	0.87	0.87	0.57	0.43	0.68	1.08	1.14	1.01
Lu	0.13	0.12	0.08	0.21	0.10	0.12	0.12	0.13	0.14	0.09	0.73	0.11	0.17	0.17	0.16

Table 2 (*Continued*)

	Fine-grained clastic rocks														
	Lower unit samples with rhombic casts, free from detrital quartz						Middle unit samples								
Analysis no.	GW98-1-19	GW98-1-21	GW98-1-22	GW98-1-23	GW98-1-25	GW98-1-26	GW99-2-21	GW99-2-22	GW99-2-23	GW99-2-24	GW99-4-19	GW99-4-20	GW99-4-21	GW99-4-23	GW99-4-24
SiO_2 (wt.%)	97.72	97.74	96.56	98.95	99.57	98.35	94.32	94.6	94.04	96.6	95.18	96.81	94.42	90.32	95.62
TiO_2	0.114	0.087	0.035	0.030	0.030	0.036	0.105	0.137	0.134	0.085	0.125	0.091	0.175	0.066	0.081
Al_2O_3	0.72	1.16	0.62	0.68	0.34	0.43	2.06	2.26	2.16	1.68	1.76	1.41	2.08	1.58	1.70
Fe_2O_3 (total)	0.24	0.15	1.80	0.04	0.11	0.08	0.26	0.06	0.38	0.11	0.11	<0.05	0.61	4.86	<0.05
MnO	<0.005	<0.005	<0.005	<0.005	<0.005	<0.005	<0.005	<0.005	<0.005	<0.005	<0.005	<0.005	<0.005	0.009	<0.005
MgO	0.02	0.01	0.01	0.01	0.01	0.01	0.01	0.02	0.02	<0.05	0.03	0.02	0.06	<0.05	<0.05
CaO	0.05	0.03	0.04	0.04	0.02	0.03	0.03	<0.05	0.01	0.02	0.02	0.02	0.02	0.02	0.02
Na_2O	0.03	0.03	0.01	0.02	0.01	0.03	0.03	0.04	0.02	0.04	0.05	0.04	0.05	0.04	0.06
K_2O	0.21	0.34	0.17	0.20	0.10	0.14	0.51	0.57	0.57	0.42	0.40	0.36	0.42	0.34	0.40
P_2O_5	0.003	0.001	0.011	0.002	0.002	0.003	0.005	0.004	0.007	0.001	0.006	0.004	0.006	0.005	0.005
H_2O (total)	0.19	0.24	0.27	0.14	0.10	0.19	0.354	0.360	0.504	0.250	0.42	0.37	0.416	0.762	0.253
Sc (ppm)	3.27	2.23	3.58	1.74	2.22	1.16	2.35	2.68	2.83	2.13	2.06	1.71	3.01	2.01	1.49
Cr	366.0	650.0	341.7	354.6	*232.6*	250	68.1	81.6	135.4	90.1	61.3	46.8	180.0	26.5	30.1
Co	0.8	0.5	1.1	0.7	0.8	0.9	n.d.	<0.5	*0.2*	<0.5	0.2	<0.5	0.4	1.2	<0.5
Rb	3.5	8.9	4.0	4.3	0.5	1.8	20.0	23.1	22.8	16.9	16.1	12.4	18.5	11.4	16.8
Sr	2.6	<0.1	<0.1	<0.1	<0.1	<0.1	12.8	2.9	<0.1	2.3	4.0	<0.1	1.1	0.2	3.0
Y	1.39	0.43	1.21	0.60	1.76	1.12	2.32	2.59	2.00	1.42	2.92	2.04	4.35	2.20	1.18
Zr	5.7	2.4	0.7	<0.1	<0.1	1.0	22	35	33	23	27	18	39	13	15.9
Ba	*94*	*112*	*73*	*36*	16	27	211	180	79	108	180	92	102	93	82
Hf							0.62	0.85	0.80	0.61	0.79	0.46	1.00	*0.33*	0.37
Ta							*0.14*	*0.15*				*0.12*	*0.16*		*0.12*
Th							1.12	1.40	1.18	0.43	1.29	0.96	1.51	1.00	1.11
U									*0.42*		*0.30*	*0.19*	*0.60*		
La (ppm)	2.80	3.69	1.16	0.76	1.32	1.33	6.87	4.48	3.46	2.45	5.27	3.00	3.87	4.70	4.78
Ce	3.22	4.00	1.85	1.10	2.36	2.09	9.81	6.92	5.39	3.96	8.98	5.47	7.01	7.69	7.69
Pr	0.35	0.51	0.23	0.13	0.30	0.26	1.04	0.74	0.56	0.41	1.05	0.61	0.75	0.85	0.79
Nd	1.26	1.35	0.96	0.52	1.33	1.13	3.44	2.60	2.02	1.47	3.85	2.29	2.89	3.04	2.63
Sm	0.27	0.15	0.23	0.12	0.35	0.27	0.56	0.46	0.35	0.26	0.65	0.43	0.60	0.52	0.39
Eu	0.09	0.04	0.09	0.05	0.14	0.11	0.15	0.13	0.09	0.08	0.16	0.11	0.19	0.13	0.09
Gd	0.30	0.11	0.27	0.15	0.43	0.31	0.42	0.41	0.31	0.20	0.51	0.36	0.62	0.45	0.27
Tb	0.04	0.01	0.04	0.02	0.06	0.04	0.06	0.06	0.05	0.03	0.08	0.06	0.10	0.06	0.04
Dy	0.25	0.08	0.21	0.11	0.34	0.21	0.39	0.42	0.34	0.22	0.48	0.35	0.68	0.38	0.22
Ho	0.05	0.02	0.04	0.02	0.06	0.04	0.08	0.09	0.08	0.05	0.10	0.08	0.15	0.08	0.05
Er	0.14	0.05	0.11	0.05	0.16	0.10	0.27	0.29	0.24	0.17	0.32	0.24	0.47	0.22	0.14
Tm	0.02	0.01	0.02	0.01	0.02	0.01	0.04	0.05	0.04	0.03	0.05	0.04	0.07	0.03	0.02
Yb	0.11	0.04	0.10	0.04	0.11	0.07	0.30	0.33	0.28	0.20	0.35	0.26	0.50	0.22	0.16
Lu	0.02	0.01	0.02	0.01	0.02	0.01	0.05	0.05	0.04	0.03	0.05	0.04	0.08	0.03	0.02

Table 2 (*Continued*)

	Barite-rich lithology												
	Lower unit			Middle unit									
Analys. no.	GW98-1-31	GW98-1-32	BMGG0201	GW99-2-16	GW99-2-17	GW99-1-20	BMGG0202	BMGG0203	MGG0242	MGG0245	MGG0246	MGG0247	MGG0248	MGG0249
SiO_2 (wt.%)	99.29	98.22	>95%	96.18	94.69	84.9	82.45	>95%	91.9	>95%	>95%	>95%	99.55	>95%
TiO_2	0.098	0.108	0.067	0.274	0.236	0.483	0.314	0.087	0.353	0.099	0.085	0.12	0.165	0.468
Al_2O_3	0.30	0.32	0.55	0.47	0.50	2.32	1.06	0.34	1.10	0.53	0.52	0.48	0.13	0.16
Fe_2O_3 (total)	0.62	2.61	0.295	1.95	1.39	7.55	17.23	2.59	7.93	2.34	1.5	1.373	1.985	1.292
MnO	0.001	0.002	<0.05	0.001	0.003	0.041	0.008	0.002	0.015	0.002	0.004	0.002	0.002	0.001
MgO	0.01	0.05	0.01	0.01	<0.05	0.16	0.03	0.002	0.02	0.02	0.02	0.01	<0.05	<0.05
CaO	0.04	0.04	0.02	0.03	0.03	0.66	0.03	0.02	0.03	0.03	0.03	0.04	0.03	0.04
Na_2O	0.03	0.02	0.05	0.02	0.02	0.06	0.05	0.04	0.02	0.01	0.01	0.01	0.01	0.01
K_2O	0.07	0.05	0.12	0.10	0.04	0.62	0.16	0.04	0.18	0.04	0.05	0.07	0.03	0.03
P_2O_5	0.028	0.027	0.014	0.016	0.013	0.027	0.035	0.009	0.021	0.013	0.011	0.009	0.017	0.023
H_2O (total)	0.13	0.33	0.133	0.26	0.33	0.74	1.32	0.33	0.61	0.39	0.28	0.21	0.19	0.26
Sc (ppm)	4.48	6.01	1.72	4.57	7.46	8.00	9.73	6.42	15.25	7.47	3.34	3.03	4.26	14.52
Cr	46.7	38.9	32.63	50.4	77.2	148.9	127	432	279.6	42.68	41.77	36.47	48.68	177.7
Co	<0.5	*0.5*	<0.5	*0.3*	*0.4*	1.7	*1.2*		0.8	*0.3*	*0.3*	<0.5	<0.5	
Rb				0.8	0.2	15.7								
Sr	2.6	0.3		<0.1	6.0	14.4								
Y	5.10													
Zr	182	288	*78*	93	250	85	243	*277*	1082	313	99	78	138	778
Ba	81	76	110	99	247	219	103	127	233	142	119	130		*153*
Hf	3.93	6.18	1.90	2.15	6.12	1.90	4.42	6.12	22.78	6.61	2.01		2.72	15.56
Ta	*0.27*	*0.32*		*0.29*	*0.35*	*0.35*			0.78	0.34	*0.18*		*0.23*	0.77
Th	2.44	2.95	1.07	2.32	4.12	4.49	5.33	3.06	11.51	3.40	2.44	1.74	4.59	13.84
U		*1.46*		*1.37*		*2.51*	*1.97*	*1.23*	*3.66*	*1.15*	*0.87*	*0.78*	*1.15*	*3.95*
La (ppm)	6.98	5.86	3.48	6.00	5.81	14.37	6.67	4.39	5.03	4.89	3.57	4.22	4.25	11.37
Ce	10.52	9.41	4.79	9.76	9.64	19.26	10.73	8.30	11.29	8.69	5.90	7.12	7.54	18.76
Pr	1.18													
Nd	3.95													
Sm	0.65	*0.77*	0.33	0.67	0.78	1.49	1.01	0.61	1.75	0.69	0.47	0.48	0.55	1.93
Eu	0.17	*0.18*		*0.15*	0.21	0.30			0.44	*0.19*	*0.11*	*0.14*	*0.15*	0.46
Gd	0.64													
Tb	0.11				*0.22*					*0.17*				*0.47*
Dy	0.77													
Ho	0.18													
Er	0.57													
Tm	0.09													
Yb	0.67	0.79	*0.22*	0.60	1.09	0.76	1.00	1.14	3.03	1.20	0.49	0.40	0.57	2.49
Lu	0.11	0.16	*0.05*	0.12	0.19	0.18	0.20	0.19	0.56	0.21	0.09	0.09	0.11	0.51

Note: Data in italics show their accuracies are low (10–20%). Others are better than 10%. Blank spaces show "not analyzed" or omitted with very low accuracy (>20%).

of selected samples were analyzed by ICP-MS in the following manner. Powdered samples of 0.3–0.5 g were weighed into PTFE beakers, into which 1–5 ml of 70% $HClO_4$ and 2–10 ml of 38% HF was added. The mixture of powdered sample and acid was heated on a hotplate at 110 °C for 3 hours and then dried at 160 °C. The samples were then dissolved in 2 ml of 1.7N HCl and centrifuged at 12,000 rpm for 10 min. The residue was added to 70–250 mg of a 3:1 flux of Na_2CO_3 and $Li_2B_4O_7$ in a platinum crucible and fused in a muffle furnace for 55 min at 900 °C. The samples were then dissolved in 6.0N HCl and centrifuged at 12,000 rpm for 10 min. Supernatant liquids were mixed with the sample obtained from the first process of HF–$HClO_4$ digestion. The solutions were dried on a hotplate at 160 °C and dissolved in 4 ml of 1.7N HCl. Matrix elements such as alkali, alkali-earth metal elements and Ba were removed from the sample solutions by the cation exchange method. The collected sample solutions were dried at 160 °C and dissolved in 2% HNO_3. Indium and Bi were used as internal standard elements. The oxide formation factor (MO^+/M^+) for each interfering LREE was determined using 20 ppb solutions, while HREE interference was corrected by applying the oxide formation factor to sample solutions. Total blank levels were lower than 1% of analytical values. The precision of REEs measurements was better than ±3%; analytical results are listed in Table 2.

We also dated detrital zircon using the U–Th–total Pb Chemical Isochron Method (CHIME) (e.g., Suzuki and Adachi, 1991; Suzuki et al., 1991). Detrital zircon grains are altered to various degrees and the ages were calculated from data obtained from portions less affected by alteration. Altered portion of zircon appears to be cloudy under the reflective microscope and can be further identified by unstable surface current during an electron microprobe analyses. Data from these altered portions were omitted from the age calculation. These results are presented in later sections.

4. Results

4.1. Major elements

Major element data indicate that the Mt. Goldsworthy clastic sedimentary rocks are composed almost exclusively of SiO_2, irrespective to rock type (Table 2). Two samples that contain relatively low SiO_2 concentrations (84.9% for GW99-1-20 and 82.5% for BMGG0202) are characterized by higher $Fe_2O_3^*$ (total Fe as Fe_2O_3) concentrations (7.55, 17.23%). Most analyzed samples have MgO, CaO and Na_2O concentrations of <0.1%. K_2O concentrations range from 0.03 to 1.27%, and show a positive correlation with Al_2O_3 (Fig. 4a). The K_2O/Al_2O_3 ratios of the five lithologies are nearly identical ($r = 0.97$ for all samples). This feature may be attributed to K-metasomatism, which is often observed in Archean sedimentary rocks and silicified volcanic rocks (e.g., Cullers et al., 1993; Fedo et al., 1996).

The average concentration of Al_2O_3 in medium-grained sandstone (MGS) is 3.23%, which is higher than the other lithologies. The coarse- to very coarse-grained sandstone (VCGS), fine-grained clastic rocks (FGC) and barite lithology (BL) have Al_2O_3 concentrations of 0.76–2.80%, 0.34–2.26% and 0.13–2.32%, respectively. Al_2O_3 concentrations in the two upper unit VCGS samples are 0.76 and 0.93%, which are lower than the 1.11–2.80% concentrations recorded in the middle and the lower units. These observations are consistent with the relatively quartz-rich and matrix-poor nature of the upper unit VCGS.

It is generally considered that Al and Ti are not fractionated relative to each other during weathering, transportation and diagenesis (Sugisaki et al., 1982; Fralick and Kronberg, 1997; Garcia et al., 1994; Young and Nesbitt, 1998). However the measured correlation between Al_2O_3 and TiO_2 is not strong ($r = 0.64$ for all samples; Fig. 4b). This result is partly due to lithology-dependent Al_2O_3/TiO_2 variation (Table 3). FGC samples record higher Al_2O_3/TiO_2 values (6.3–23.9 with an average of 16.1) than VCGS (7.1–16.1 with an average of 10.9) and MGS (4.0–12.2 with an average of 8.6). The BL samples occasionally record very low values, 0.4–8.2, with an average of 3.6. Variation in Al_2O_3/TiO_2 within each lithology should also be considered as an explanation for the poor correlation between TiO_2 and Al_2O_3.

4.2. Minor elements

4.2.1. High field strength and transition elements

With the exception of BL samples, MGS is the lithology most enriched in high field strength elements (HFSE) (Zr, Th, Hf, Ta). For example, Zr concentration in MGS varies from 49 to 241 ppm, with an average of 107 ppm. In comparison, VCGS and FGC record Zr concentrations ranging from 27 to 84 ppm (average 47 ppm) and from <1 to 39 ppm, respectively. A similar trend can be seen for Th (0.66–3.29 ppm for VCGS, 0.98–4.29 for MGS, and 0.43–1.51 ppm for FGC). The BL samples are characterized by very high concentrations of HFSE; Zr, Th and Hf concentrations are up to 1000, 14 and 23 ppm, respectively.

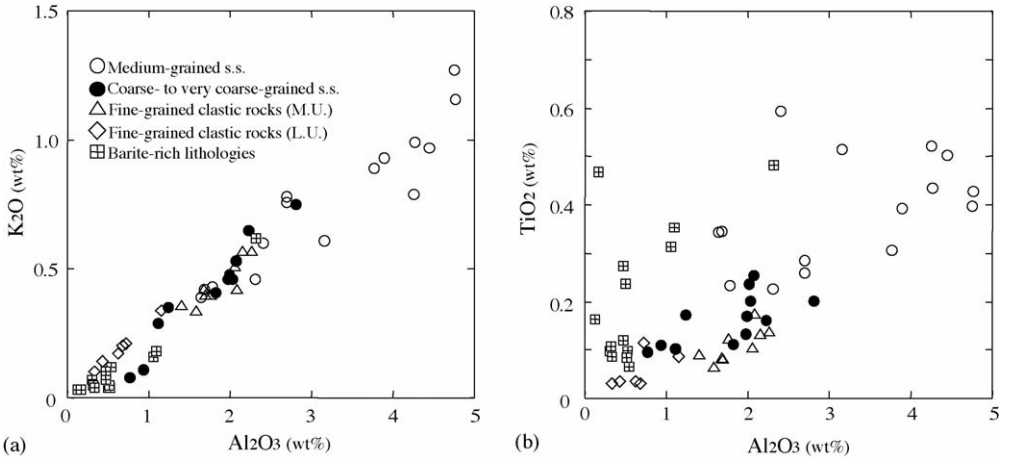

Fig. 4. (a) Al_2O_3 plotted against K_2O. (b) Al_2O_3 plotted against TiO_2. Open circles: medium-grained sandstone; black circles: coarse- to very coarse-grained sandstone; open triangles: fine-grained sandstone from the middle unit; open diamonds: fine-grained sandstone from the lower unit; open squares with internal cross: barite-rich lithologies.

Scandium shows a similar trend to HFSE. Scandium concentrations are higher in MGS (3.8–7.4 ppm) than VCGS (1.5–3.8 ppm) and FGC (1.2–3.6 ppm). Two of the BL samples record Sc > 10 ppm. Chromium concentrations are similar in MGS (38–125 ppm with an average of 83 ppm) and FGC from the middle unit (26–180 ppm with an average of 80 ppm). VCGS contains a relatively low concentration of Cr (22–76 ppm with an average of 43 ppm) compared to other lithologies. FGC within the lower unit is characterized by high

Table 3
Total REE and some selected geochemical indices for Mt. Goldsworthy siliciclastic rocks

	Very coarse to coarse-grained s.s.			Medium-grained sandstone (L.U.)			Medium-grained sandstone (M.U.)		
	Average	Range	*n*	Average	Range	*n*	Average	Range	*n*
∑REE	10.90	–	1	23.01	15.50–29.61	6	32.97	14.58–51.96	9
Al_2O_3/TiO_2	10.9	7.1–16.1	12	6.86	4.0–10.4	6	9.80	6.1–12.2	9
Cr/Th	29.8	16.3–82.9	12	28.47	17.7–37.3	6	41.31	21.46–127.6	9
Th/Sc	0.71	0.27–1.27	12	0.49	0.39–0.57	6	0.53	0.27–0.75	9
Cr/Zr	0.87	0.58–1.61	12	0.61	0.31–0.96	6	1.12	0.66–2.55	9
La/Sc	1.45	1.02–2.53	12	1.11	0.62–1.61	6	1.73	1.16–2.57	9
La/Sm(*n*)	4.52	3.66–5.50	12	5.10	4.29–6.27	6	5.72	4.48–8.75	9
Gd/Yb(*n*)	0.95	–	1	0.78	0.60–1.26	6	0.92	0.79–1.02	8
La/Yb(*n*)	5.90	2.75–7.05	12	4.86	3.37–7.56	6	7.53	5.69–12.21	9
Eu/Eu*	0.90	–	1	0.92	0.88–1.03	6	0.76	0.72–0.80	8

	Fine-grained clastic rocks (L.U.)			Fine-grained clastic rocks (M.U.)			Barite-rich lithology		
	Average	Range	*n*	Average	Range	*n*	Average	Range	*n*
∑REE	6.73	3.09–10.07	6	16.91	9.56–23.48	9	26.59	–	1
Al_2O_3/TiO_2	13.87	6.3–22.7	6	17.6	11.9–23.9	9	3.55	0.4–8.2	14
Cr/Th	–			79.2	26.5–209.5	9	28.57	10.6–141.3	14
Th/Sc	–			0.51	0.2–0.74	9	0.63	0.46–1.08	14
Cr/Zr	268.30	64.2–488	4	2.98	1.89–4.62	9	0.53	0.14–1.75	14
La/Sc	0.84	0.32–1.65	6	2.01	1.15–3.21	9	1.07	0.33–2.02	14
La/Sm(*n*)	5.75	2.36–15.42	6	5.86	4.04–7.69	9	4.87	1.80–6.73	14
Gd/Yb(*n*)	2.79	2.23–3.66	6	1.15	0.83–1.69	9	0.79	–	1
La/Yb(*n*)	20.69	8.03–63.87	6	11.28	5.36–20.68	9	5.64	1.15–13.09	14
Eu/Eu*	1.05	0.90–1.15	6	0.87	0.80–1.03	9	0.79	–	1

Note: L.U., lower unit; M.U., middle unit; *n* shows number of data.

Cr concentrations (230–650 ppm). Cobalt concentration is very low (<2 ppm) in all lithology types.

Fig. 5 shows Zr–Th, Zr–Hf and Cr–Sc relationships for all analyzed samples. A clear positive correlation ($r > 0.9$) is evident for Zr–Th and Zr–Hf that commonly show higher concentrations in felsic rocks than in mafic to ultramafic rocks. Relationships between mafic components (Cr and Sc) are less clear, which may reflect lithological variation. If FGC samples are excluded, the correlation coefficient between Cr and Sc is 0.70.

Averages and ranges for the HFSE and transition element ratios most useful for provenance analysis are shown in Table 3. The Cr/Th, Th/Sc ratios of most of lower unit FGC samples cannot be calculated due to very low Th concentrations (<0.5 ppm), whereas Cr/Zr ratios are identical to that of ultramafic rocks (Cr/Zr ≥ 75 for komatiite). Other lithologies record Cr/Th, Th/Sc and Cr/Zr ratios similar to those of Archean tonalite, or the transition between tonalite and basalt (Cr/Th = 6.5, Th/Sc = 1.3 and Cr/Zr = 0.3 for tonalite; Cr/Th = 500, Th/Sc = 0.02 and Cr/Zr = 5.5 for basalt) (Condie and Wronkiewicz, 1990).

4.2.2. Rare earth elements (REEs)

Chondrite-normalized REE patterns from the Mt. Goldsworthy sedimentary rocks vary systematically in relation to lithology and stratigraphy (Fig. 6; Table 3). Lower unit VCGS and MGS samples are characterized by fractionated LREE and enrichment in HREE (Fig. 6a and b). Middle unit VCGS samples, with the exception of sample GW93-1-2, record a steady decrease from La to Yb, whereas the two upper unit samples and sample GW93-1-2 record a V-shaped pattern (Fig. 6a). It is possible that the two upper unit samples and GW93-1-2 have a negative Eu anomaly, although Eu/Eu^* cannot be calculated due to a lack of Gd data. Middle unit MGS samples commonly display a negative Eu anomaly ($Eu/Eu^* = 0.72–0.80$), and are characterized by highly fractionated LREE ($La/Sm(n) \geq 4.5$) and an approximately flat trend from Gd to Lu or slight HREE enrichment ($Gd/Yb(n) = 0.79–1.02$; Fig. 6c). Lower unit FGC samples display a steady decrease from La to Lu with a slight positive Eu anomaly for some samples ($Eu/Eu^* \geq 1.1$; Fig. 6d). Middle unit FGC samples display a smooth decrease from La to Sm, variable MREE to HREE concentrations ($Gd/Yb(n) = 0.83–1.69$), and a slight negative Eu anomaly ($Eu/Eu^* \leq 0.9$; Fig. 6e).

Chondrite-normalized REE patterns of BL samples can be divided into two types: those with a low abundance of REE and a relatively flat pattern from La to Lu (the presence of an Eu anomaly is not known), and those

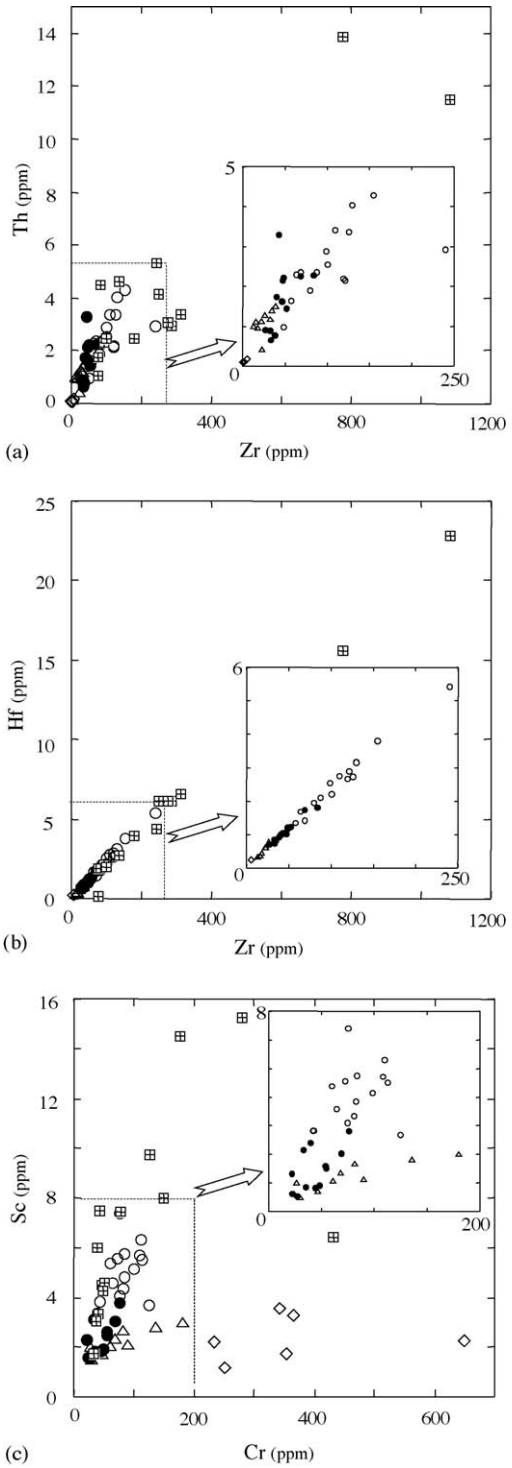

Fig. 5. (a) Zr plotted against Th; (b) Zr plotted against Hf; (c) Cr plotted against Sc. See Fig. 4 for key to symbols.

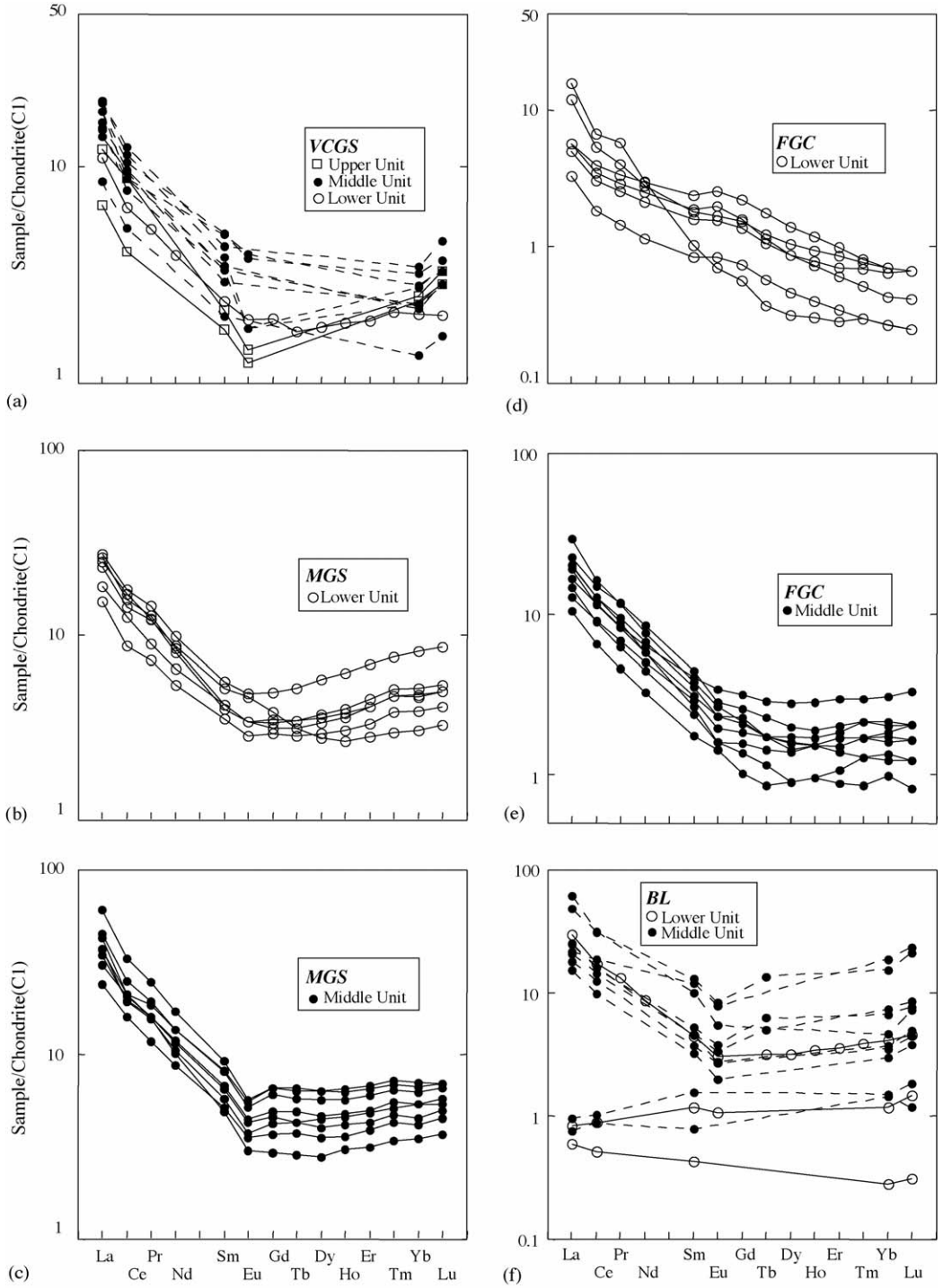

Fig. 6. Chondrite(C1)-normalized REE patterns for Mt. Goldsworthy lithologies. Data shown in (a), except for lower unit sample and (f) were measured by INAA, all other data by ICP-MS.

with fractionated LREE and a potentially pronounced negative Eu anomaly. Weak positive or negative fractionation trends from Gd to Yb are apparent in some samples.

4.2.3. Characteristics of Rb and Ba

Rubidium concentrations vary from <0.5 ppm (the approximate detection limit) to 46 ppm, and show a strong positive correlation with K_2O ($r = 0.96$ for all

samples analyzed for K and Rb). Barium concentrations range from 16 to 623 ppm and show a weak position correlation with Al_2O_3 ($r = 0.62$).

5. Discussion

5.1. Effect of post-depositional alteration (silicification) on sediment geochemistry

The high SiO_2 concentrations and replacement of lithic fragments by microcrystalline quartz indicate that the Mt. Goldsworthy metasedimentary rocks were subjected to silicification. Silicification is widely observed in greenstone belts of the Pilbara Craton and other Archean greenstone belts (Cullers et al., 1993; DiMarco and Lowe, 1989a; Duchač and Hanor, 1987; Hanor and Duchač, 1990; Lowe, 1999; Lowe and Byerly, 1986; Lowe and Knauth, 1977; Paris et al., 1985; Van Kranendonk, 2006; Van Kranendonk and Pirajno, 2004).

Silicification is thought to result from either post-depositional hydrothermal alteration or syndepositional interaction with seawater at low-temperatures, or some combination of the two processes (Lowe, 1999; Van Kranendonk, 2006, and references therein). In either case, protolith chemical composition is altered during silicification; most of Ca, Mg and Na, and to a lesser extent Fe, Mn and Sr is removed, whereas Si and occasionally K are added (Cullers et al., 1993; Van Kranendonk and Pirajno, 2004). These trends are apparent in the Mt. Goldsworthy samples (Table 2). HFSE (Zr, Ti, Th, Nb and Ta), Cr, Sc, Al and REEs, on the other hand, are generally regarded as immobile during silicification. In particular, Zr and Ti are representatives of the least mobile elements (Cullers et al., 1993; Lowe, 1999; Polat et al., 2002; Polat and Hofmann, 2003, and references therein), although under peculiar conditions these two elements could be mobile (Salvi and Williams-Jones, 1996). Relationship between Zr and Ti in the Mt. Goldsworthy samples is not always strongly positive, due to significant variation of Zr/Ti ratios of BL (Fig. 7). If BL samples are excluded, there is a strong positive correlation between Zr and Ti ($r = 0.89$). Furthermore Th, Sc, Al and REEs show a strong positive correlation with Zr and/or Ti ($r > 0.8$), contrastive to low correlation coefficient for mobile elements such as Fe ($r = 0.02$ and 0.14 for Fe–Ti and Fe–Zr, respectively). Such the inter-element positive correlations of these so-called immobile elements, except Cr, suggest that they were not significantly fractionated during post-depositional events including alteration and diagenesis. Correlation coefficients for Cr–TiO_2 and Cr–Zr are 0.28 and 0.33, respectively. Chromium appears to be less immobile compared with the others, although it shows moderately positive correlation with Sc for some sample groups (Fig. 5C).

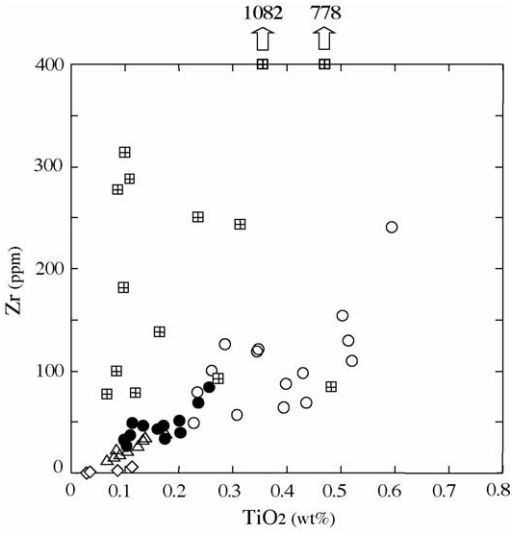

Fig. 7. TiO_2 plotted against Zr. See Fig. 4 for key to symbols.

The immobile elements (HFSE, Sc, Al and REEs) might have been reduced in concentration by the substantial addition of Si during silicification; however, their inter-element relationships (e.g. ratios and patterns normalized to given standards such as chondrite) are mostly preserved. We therefore conclude that the immobile elements can be used as powerful and reliable tools for provenance analysis of Mt. Goldsworthy clastic sedimentary rocks.

5.2. Factors controlling the geochemistry of Mt. Goldsworthy clastic sedimentary rocks

5.2.1. Al–Ti–Zr fractionation

Al_2O_3/TiO_2 ratios in igneous rocks generally vary according to rock type, although this ratio is not as sensitive as Cr/Th or Th/Sc (Condie and Wronkiewicz, 1990). The Al_2O_3/TiO_2 ratio of felsic igneous rocks is generally >10 and can be >100. Mafic and ultramafic rocks, on the other hand, tend to record ratios <20, although they rarely have Al_2O_3/TiO_2 ratios larger than 50 (Byerly, 1999). Al-depleted high MgO-rocks possibly have the lowest value of around 4 (e.g. Sugitani et al., 1996). Al_2O_3/TiO_2 ratios in sedimentary rocks can therefore be used as a primary indicator of source rock type.

Although the available geochemical data from Archean sandstone is limited compared with shale lithologies, the majority of published Al_2O_3/TiO_2 ratios

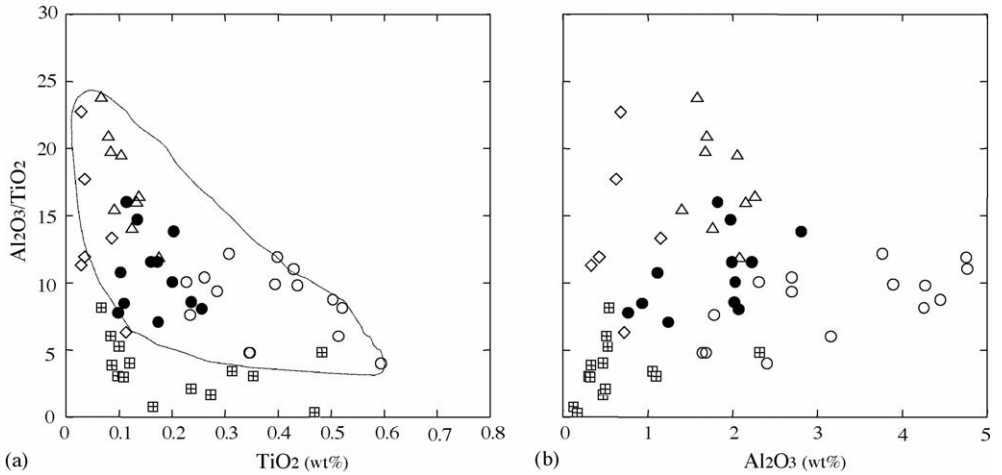

Fig. 8. (a) Al_2O_3/TiO_2 plotted against TiO_2. (b) Al_2O_3/TiO_2 plotted against Al_2O_3. See Fig. 4 for key to symbols. Note that the BL and other lithologies independently define an inverse relationship between Al_2O_3/TiO_2 and TiO_2.

are >10 (Taylor and McLennan, 1985; Condie, 1993; Naqvi et al., 2002; Kato and Ikezaki, 2000; Wronkiewicz and Condie, 1989), and many are in the range of 20–50, corresponding to intermediate to felsic rocks. In contrast, the Mt. Goldsworthy clastic sedimentary rocks, in particular VCGS, MGS and BL, are characterized by low Al_2O_3/TiO_2 ratios in the range of 0.4–16.1. Some samples have an anomalously low Al_2O_3/TiO_2 value (<4; the assumed lowest value for igneous rocks) (Table 3). FGC, MGS and VCGS samples cooperatively show an inverse relationship between TiO_2 and Al_2O_3/TiO_2, while there is no clear relationship between Al_2O_3 and Al_2O_3/TiO_2 for these groups (Fig. 8). These relationships suggest that lower Al_2O_3/TiO_2 values are accompanied by enrichment of Ti. The relationship between TiO_2 and Zr (Fig. 7) indicates that Ti-enrichment is also associated with Zr concentration. Similarly BL samples generally show an inverse relationship of TiO_2 with Al_2O_3/TiO_2 and a positive relationship of TiO_2 with Zr (Figs. 7 and 8), although they plot out of the trend of the other lithologies.

The geochemical trend described above is consistent with the observation that samples often contain laminae enriched in heavy minerals such as zircon and Fe–Ti oxides (Fig. 3c). As shown below, there is no evidence for the formation of the Ti- and Zr-rich laminae by mechanical maturation of sediment. Within MGS, the zircon and Fe–Ti oxide-rich laminae are occasionally set in poorly sorted and relatively matrix-rich sandstone (Fig. 3c). The BL is composed of bladed barite crystals and detrital barite that are inter-layered or admixed with terrigenous detritus including quartz, Ti-oxides, zircon and angular lithic fragments (Fig. 3d–f). Namely, the formation of laminae likely resulted from sediment flow enriched in these resistant heavy minerals rather than the result of prolonged in situ abrasion and sorting. In a later section, the origin of the Ti- and Zr-enriched and relatively Al-depleted sediment will be discussed in the context of hydrothermal alteration and chemical weathering in the source region.

5.2.2. Factors controlling REE geochemistry

5.2.2.1. HREE-enrichment. The remarkable V-shaped REE pattern of Mt. Goldsworthy clastic sediments is highly unusual (Fig. 6). The REE pattern can be interpreted as resulting from the mixing of two end-member materials: one LREE-enriched and another HREE-enriched. This interpretation is supported by the relationships between Al_2O_3, Zr, La and Yb (Fig. 9). Lanthanum shows a stronger correlation with Al_2O_3 ($r = 0.77$) than with Zr ($r = 0.51$), while Yb shows a clear positive correlation with Zr ($r = 0.92$) and a weaker correlation with Al_2O_3 ($r = 0.65$) than La. These data suggest that different phases host La and Yb within the sediment.

Zircon, an Al-free silicate, is the principal host mineral for Zr in sedimentary and igneous rocks, and is common within the Mt. Goldsworthy samples. Zircon tends to be HREE-enriched, with highly fractionated Sm–Yb and occasionally a pronounced negative Eu anomaly (e.g., Heaman et al., 1990; Whitehouse and Kamber, 2003). We therefore suggest that detrital zircon contributes significantly to the HREE content of the bulk sediments; this idea is further confirmed by the inverse correlation of Sm/Yb(n) with Zr/Al_2O_3 (Fig. 10). An additional host phase for REEs is composed of aluminosilicates such as clays, micas and feldspars that as a whole have REE patterns characterized by LREE-enrichment. Namely these two components control the REE geochemistry of the Mt. Goldsworthy clastic rocks.

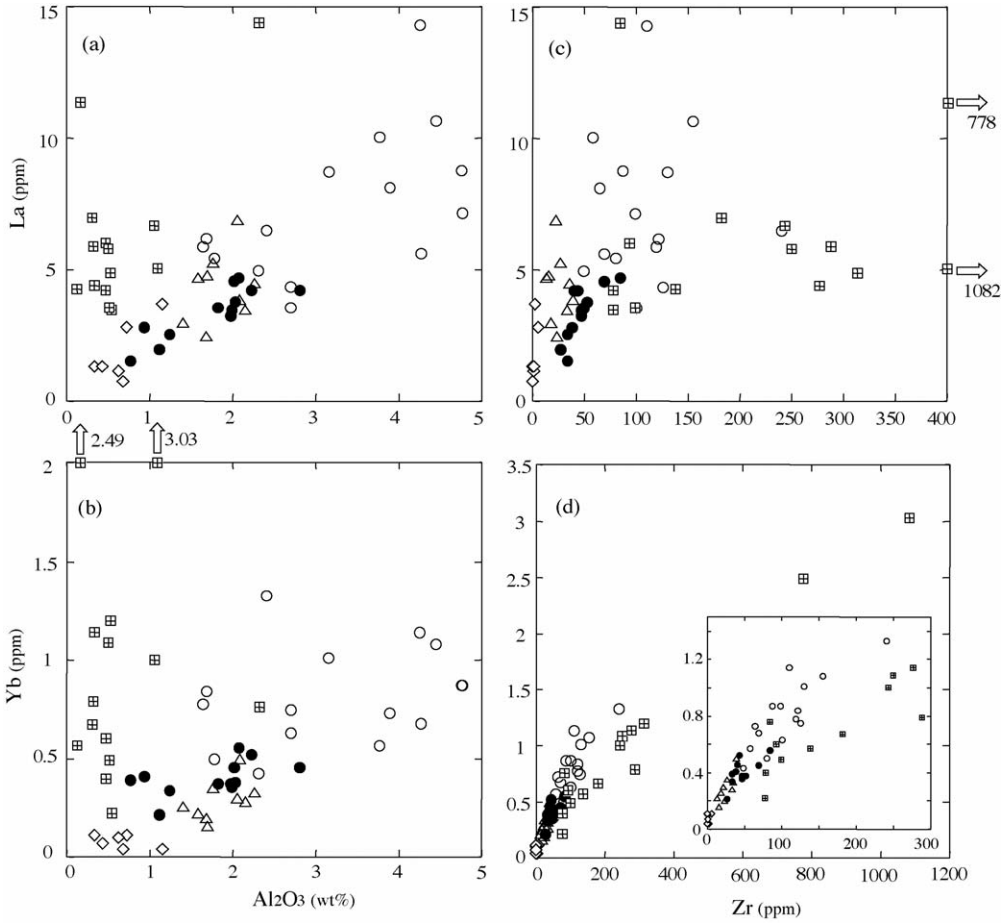

Fig. 9. (a) Al_2O_3 plotted against La; (b) Al_2O_3 plotted against Yb; (c) Zr plotted against La; (d) Zr plotted against Yb. See Fig. 4 for key to symbols.

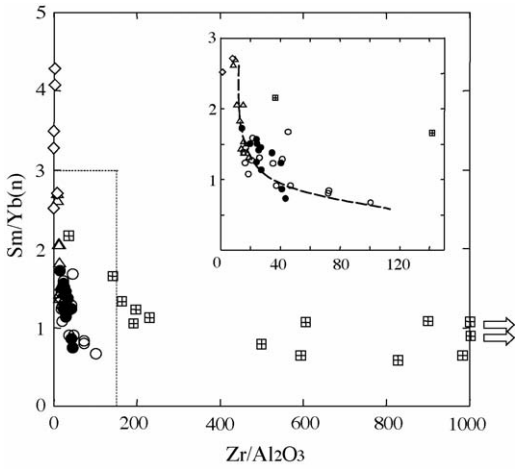

Fig. 10. Zr/Al_2O_3 plotted against Sm/Yb(n). See Fig. 4 for key to symbols.

This model can be tested by REE data of zircon and comparison of La and Yb contents between Zr-enriched and -depleted samples (GW99-5-3 with 241 ppm of Zr and GW99-4-24 with 15.9 ppm of Zr, respectively); here we use GW99-4-24 as an equivalent to aluminosilicate fraction. In the following calculation, 20 ppm of La and 1000 ppm of Yb are taken as values in zircon, based on data from Heaman et al. (1990). Additionally we assume that 95% of Zr in the sample GW99-5-3 was supplied as detrital zircon, from the comparison of Zr data between GW99-5-3 and GW99-4-24. Concentrations of La and Yb contained in zirconium fraction in GW99-5-3 are consequently calculated to be 0.009 and 0.46 ppm, respectively. Although this calculated value of Yb (0.46 ppm) is somewhat lower than the analyzed value in GW99-5-3 (1.33 ppm), this result indicates influx of detrital zircon could affect significantly Yb concentration, but not La in bulk sediments, because concentration of La and Yb in GW99-4-24 are 4.78 and 0.16 ppm, respectively.

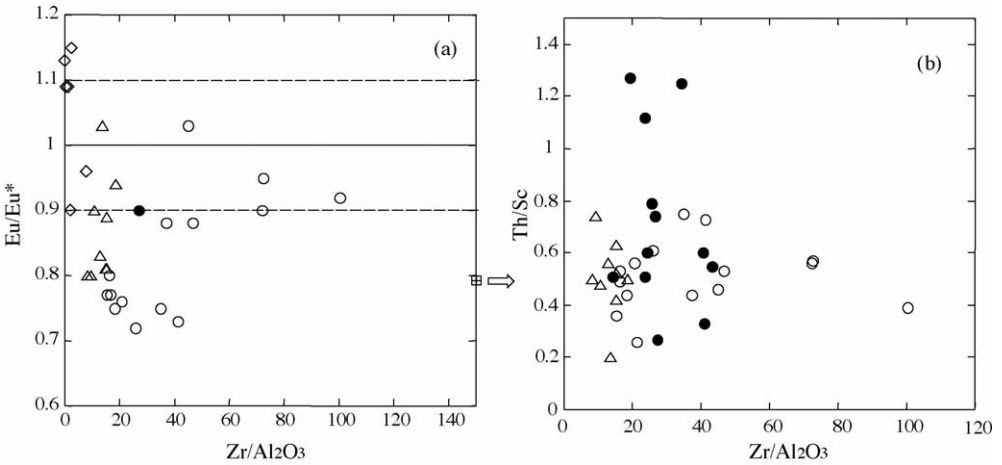

Fig. 11. (a) Zr/Al_2O_3 plotted against Eu/Eu^*; (b) Zr/Al_2O_3 plotted against Th/Sc. See Fig. 4 for key to symbols.

5.2.2.2. Eu anomaly. Many of the MGS samples display a negative Eu anomaly ($Eu/Eu^* < 0.9$; Table 3). We also assume that the VCGS and BL samples have a negative Eu anomaly. Additionally, some middle unit FGC samples display a negative Eu anomaly, whereas those from the lower unit do not. Several lower unit FGC samples show a slight positive Eu anomaly ($Eu/Eu^* > 1.1$). Negative Eu anomalies have been of special interest in the provenance study of Archean rocks because the anomaly is considered to indicate the presence of granitic source rocks (Condie, 1993; Cullers and Podkovyrov, 2002; Fedo et al., 1996; Gao and Wedepohl, 1995; Kato and Ikezaki, 2000; Taylor and McLennan, 1985). In this study, we are cautious in interpreting the negative Eu anomaly because zircon, which has a pronounced negative Eu anomaly, is locally accumulated within the sediments. In order to illustrate this point, we have plotted the samples on a Zr/Al_2O_3–Eu/Eu^* plot (Fig. 11). There is no clear relationship between Zr/Al_2O_3 and Eu/Eu^*, which indicates that Eu/Eu^* ratios probably reflect the source rock type.

5.3. Provenance of Mt. Goldsworthy clastic sedimentary rocks

5.3.1. Implications of bulk sediment geochemistry

In this section we discuss in detail the provenance of VCGS and MGS from the lower and middle units and FGC from the upper unit. FGC from the lower unit was previously interpreted as derived from a mafic to ultramafic source by Sugitani et al. (2003), based on Cr–Al–Zr–Ti systematics. The present study, on the other hand, reveals that they show a positive Eu-anomaly and a significant fractionation between LREE and HREE (Fig. 6d), unlike mafic to ultramafic rocks. As described in Sugitani et al. (2003), the rocks contain abundant silicified rhombic crystals that originated from authigenic carbonate. Therefore, REE incorporated originally in this authigenic phase may remain and surpass the REE signature of clastic components largely derived from a mafic to ultramafic source. BL samples contain significant amounts of reworked barite and other unidentified precipitate, which may have significantly modified trace element signatures related to clastic components. As discussed in the later section, the BL samples probably reflect directly the nature of the hydrothermally altered zone of the source region. Therefore, FGC from the lower unit and BL are excluded from the following discussion.

The provenance of Mt. Goldsworthy clastic sedimentary rocks is examined, based on the distribution patterns of Zr/Al_2O_3–Th/Sc, Th/Sc–La/Sc and Eu/Eu^*–Th/Sc. Elements used for these discrimination diagrams are basically regarded as immobile during post-depositional alteration in the present case, as discussed earlier. Zr/Al_2O_3–Th/Sc relationships are introduced to demonstrate that alteration and mineralogy have had negligible effect on provenance analysis. The Zr/Al_2O_3–Th/Sc relationship tests the influence of the local accumulation of heavy minerals on Th/Sc ratios. There is no systematic relation between Th/Sc and Zr/Al_2O_3 ratios ($r = 0.036$; Fig. 11b). We conclude therefore, that the Th/Sc ratio, a key indicator of provenance, is not affected by the local accumulation of heavy minerals represented by zircon.

In terms of the Th/Sc–La/Sc relationship, the Mt. Goldsworthy rocks plot in the region between Archean average tonalite–trondhjemite–granodiorite (TTG) and

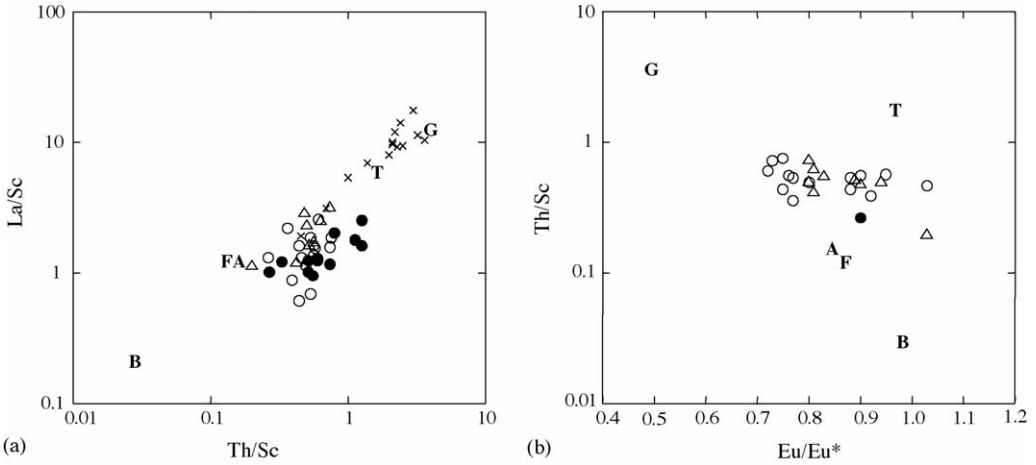

Fig. 12. (a) Th/Sc plotted against La/Sc; (b) Eu/Eu* plotted against Th/Sc (after Cullers and Podkovyrov, 2002). See Fig. 4 for key to symbols. Crosses in (a) are volcanic and volcaniclastic rocks of the Panorama Formation (Cullers et al., 1993). G: granite; T: tonalite–trondhjemite–granodiorite; F: felsic volcanic rock; A: andesite; B: basalt. Data for average values of Early Archean igneous rocks are sourced from Condie (1993).

felsic volcanics and andesite (Fig. 12a). The Th–Sc–La system provides clear geochemical evidence that the detrital material was derived at least partially from TTG or granitic sources. The mixing of TTG- or granite-derived detrital material with mafic-derived material explains the geochemical characteristics of the Mt. Goldsworthy rocks. Neither andesite nor felsic volcanics can be considered a unique mixing end-member. The petrological features (Table 1; Fig. 3) clearly demonstrate the mixed provenance of three or more components including sedimentary rocks and mafic to ultramafic volcanic rocks. The Eu/Eu*–Th/Sc relationship (Fig. 12b) may provide more specific information concerning the provenance of Mt. Goldsworthy rocks. Half of the analyzed samples, including both FGC and MGS samples, plot in the region suggesting the contribution of granitic source rocks.

5.3.2. CHIME geochronology of detrital zircon

We used the CHIME method (Suzuki and Adachi, 1991; Suzuki et al., 1991) to determine the ages of two detrital zircons from clastic layers associated with lower unit black chert. The two detrital zircon grains yielded ages of 3.67 ± 0.16 and 3.71 ± 0.12 Ga (Fig. 13). The first data is similar to the age of the oldest rock in the Pilbara Craton, an inclusion of gneissic tonalite from the Warrawagine Granitoid Complex (3.57–3.65 Ga), whereas the second data is close to the oldest date (>3.72 Ga) for a recycled xenocrystic zircon in the Panorama Formation (Thorpe et al., 1992; Van Kranendonk et al., 2002, and references therein).

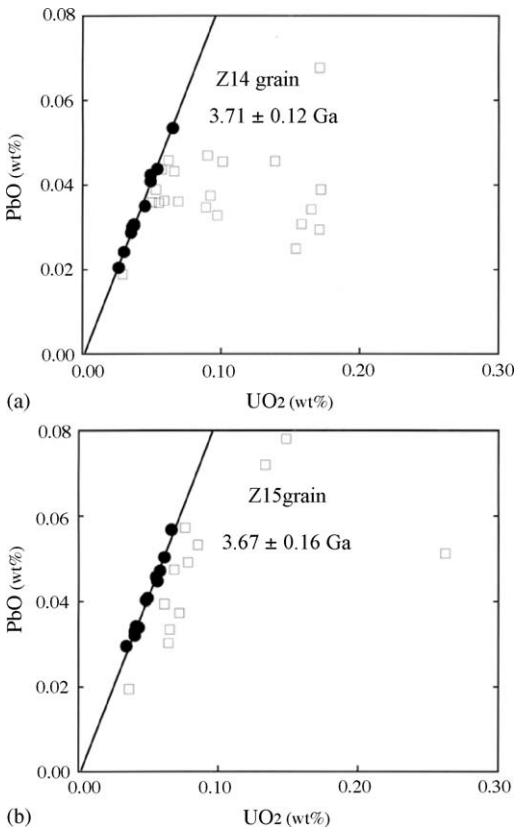

Fig. 13. Plots of PbO vs. corrected UO_2 (UO_2 plus the equivalent of ThO_2) for two detrital zircon grains from the alteration of chert and sandstone in the lower unit (including chert breccia; also see Fig. 2). Note that the zircon grains were subjected to alteration. Open squares show data from relatively porous and cloudy altered portions, whereas closed squares show data for clear portions less affected by alteration, in the same zircon grain.

6. Synthesis and implications

6.1. Alteration of source rocks—implications of hydrothermal activity

Sugitani et al. (1996) reported anomalously low Al_2O_3/TiO_2 ratios (<4) for Archean silicified fine-grained clastic sediments from Point Samson in the West Pilbara Granite–Greenstone Terrane of the Pilbara Craton. The low Al_2O_3/TiO_2 ratios were interpreted as a result of supply of Ti- and Zr-enriched and Al-depleted detrital material to the site of sediment deposition. Such detrital materials were interpreted produced by intense chemical weathering of source rocks that accelerated Al–Ti fractionation, Al-removal and Ti-retention. Several authors emphasize intense chemical weathering during the Archean under high surface temperature, high CO_2 partial pressure, and/or significant emission of acidic volcanogenic products such as SO_x and HCl (e.g., Lowe and Tice, 2004; Sugitani et al., 1996, and references therein), whereas others report minor chemical weathering (e.g., Hofmann, 2005).

As described earlier, the Mt. Goldsworthy clastic sedimentary rocks are similar to the Point Samson rocks. Al_2O_3/TiO_2 values are variable and occasionally very low (<4) due to an influx of Ti-rich detritus. Mt. Goldsworthy metasedimentary succession also includes quartz-rich sandstone, including quartz arenite. The origin of Archean quartz-rich sandstone is often ascribed to intense chemical weathering (Corcoran et al., 1998, 1999; Donaldson and de Kemp, 1998). Thus, the data presented in this study may provide geochemical and petrological evidence for intense chemical weathering during the Archean. However, it may be significant that the Mt. Goldsworthy sandstones contain silicified lath-shaped sericite pseudomorphs after feldspar. Sugitani et al. (2003) noted that abundant well-rounded mono-crystalline detrital quartz in the Mt. Goldsworthy succession might not be evidence for intense chemical weathering in the source region. The quartz grains are associated with feldspar laths (Fig. 3b), and the preservation of labile detrital feldspar laths would exclude the possibility that the source area was subjected to prolonged intense chemical weathering (e.g., Nesbitt et al., 1997 and references therein). Well-rounded quartz grains are therefore considered more likely to represent recycled material from older quartz-rich sediment.

If the above interpretation is correct, then we still must explain the origin of Al-depleted and Zr- and Ti-enriched detrital material within the Mt. Goldsworthy clastic sedimentary rocks. As a hypothesis, we propose that Zr- and Ti-enriched detrital materials were formed by hydrothermal alteration of the sediment source area, under the acid condition (pH < 4). Hydrothermal discharge zone was likely located proximal to the source of terrigenous detrital material, probably at a subaerial setting, because some of the Zr- and Ti-enriched detrital materials were transported by an intermittent high-energy flow and the shallow to subaerial depositional environment of the middle unit is suggested (Sugitani et al., 2003). Mixture of the detrital materials with non-altered detritus produced the highly variable and occasionally very low Al_2O_3/TiO_2 values. This model is not unrealistic, because hydrothermal activity on land has been reasonably common phenomenon in the Archean, like today.

The subaerial hydrothermal alteration model described above would give some implication of authigenic barite ($BaSO_4$) formation. Due to its low solubility in a wide range of pH (Brookins, 1988), barite formation, if not all, could be explained by mixing of SO_4^{2-}-rich solution and Ba^{2+}-rich one. As previously proposed by Sugitani et al. (2003), it is possible that the SO_4^{2-}-rich solution was seawater, whereas the Ba^{2+}-rich solution was hydrothermal one, with significantly low pH. Alternatively, barite may have been precipitated from a hydrothermal solution originally enriched in both Ba^{2+} and H_2S. After a subaerial discharge, H_2S in the hydrothermal solution has been photochemically oxidized to produce SO_4^{2-}, which reacted with Ba^{2+} to precipitate barite. Oxidation of H_2S also resulted in acidification of the solution, which resulted in intense alteration of surrounding rocks and/or sediments and produced Ti- and Zr-enriched and Al-depleted detrital materials. This model could explain why the BL samples plot out of the general trend in many of the geochemical plots presented in this study (Figs. 7–10), and proposes a new process of barite formation in the Archean, while many other Archean barite deposits have been interpreted to be seafloor or sub-seafloor hydrothermal deposits (Heinrichs and Reimer, 1977; Lowe and Knauth, 1977; Nijman et al., 1998; Pirajno and Grey, 2002; Pirajno and Van Kranendonk, 2005; Van Kranendonk and Pirajno, 2004; Van Kranendonk, 2006).

6.2. Source of Mt. Goldsworthy clastic sedimentary rocks

As suggested in former Section 5.3.1 focused to provenance, geochemical characteristics of Mt. Goldsworthy clastic sedimentary rocks indicate contribution of TTG- and/or granite-derived felsic detrital

material and mafic to ultramafic one. The Warrawoona mafic to ultramafic suites including the underlying heavily altered volcanic to volcaniclastic rocks could be potential source for mafic to ultramafic detrital materials. Source of felsic components, on the other hand, is still unclear. One potential source is the Panorama Formation, which was subjected to regional sub-aerial erosion and locally overlain by the Strelley Pool Chert (Van Kranendonk et al., 2002). The distribution pattern in the Th/Sc–La/Sc plot (Fig. 13a) also suggests that the formation could be one of the end-members of provenances for the Mt. Goldsworthy rocks. This interpretation is however tentative because the felsic flow rocks and volcaniclastic sandstone and siltstone from the Panorama Formation did not yet record negative Eu anomalies (Cullers et al., 1993). The 3.47 Ga Duffer Formation, a lower unit than the Panorama Formation, displays a distinctive negative Eu anomaly ($Eu/Eu^* = 0.61$; Jahn et al., 1981), although evaluation of this formation as a potential detrital source is not possible due to insufficient data. In either case, the age of detrital zircon in the Mt. Goldsworthy sediments (3.67 ± 0.16 and 3.71 ± 0.16 Ga; Fig. 13) requires detrital sources older than both the Panorama and the Duffer Formations. The petrography, in particular abundant well-rounded monocrystalline quartz also favors a mixed and recycled source for Mt. Goldsworthy clastic sedimentary rocks.

The emergent block of continental crust was probably exposed in the Pilbara Craton probably at ~3.5 Ga (Buick et al., 1995; Thorpe et al., 1992). This is supposed by geochemistry and geology of basalt and komatiite in the Warrawoona Group (Green et al., 2000; Van Kranendonk and Pirajno, 2004; Smithies et al., 2005) and of shale and sandstone associated with the Marble Bar Chert (Kato and Ikezaki, 2000). The results of the present study provide further evidence for the early (>3.5 Ga) evolution and recycling of continental crust in the Pilbara Craton.

7. Conclusions

We undertook a geochemical and petrological study of Archean silicified clastic sedimentary rocks in the Mt. Goldsworthy region, Pilbara Craton, Western Australia, to investigate the early evolution of continental crust and the nature of surface weathering and alteration. The Mt. Goldsworthy sedimentary succession is assigned to the Kelly Group and is interpreted to be a correlative of the 3.43 Ga Strelly Pool Chert.

The bulk geochemistry of Mt. Goldsworthy clastic sedimentary rocks is controlled by source rock composition and the inflow of Zr- and Ti-enriched detrital material. These unusual detrital materials formed locally in the source region by Al-dissolution and residual Ti- and Zr-enrichment under acidic ($pH < 4.0$) conditions. Alteration has possibly been related to hydrothermal activity and barite precipitation.

Conservative geochemical indicators (Th/Sc, La/Sc and Eu/Eu^*), petrological features and CHIME ages of detrital zircon clearly demonstrate the mixed provenance and recycling of detrital material contained within the Mt. Goldsworthy clastic sedimentary rocks. These data also support the early (>3.5 Ga) evolution of the continental crust, including granite formation.

Acknowledgments

We especially wish to express our gratitude to Dr. R. Sugisaki, Meijo University and Dr. Nagamine, Nagoya University who helped us with sampling. Informal review by Dr. M. Van Kranendonk, the Geological Survey of Western Australia is appreciated. We also acknowledge two anonymous reviewers for their critical and constructive comments. This work was supported by the Joint Research Program (Japan-Australia), the Japan Society of the Promotion of Science.

References

Barley, M.E., 1993. Volcanic, sedimentary and tectonostratigraphic environments of the ~3.46 Ga Warrawoona Megasequence: a review. Precambrian Res. 60, 47–67.

Bhatia, M.R., Crook, K.A.W., 1986. Trace element characteristics of graywackes and tectonic setting discrimination of sedimentary basins. Contrib. Mineral. Petrol. 92, 181–193.

Brookins, D.G., 1988. Eh-pH Diagrams for Geochemistry. Springer-Verlag, Berlin.

Buick, R., Thornett, J.R., McNaughton, N.J., Smith, J.B., Barley, M.E., Savage, M., 1995. Record of emergent continental crust ~3.5 billion years ago in the Pilbara craton of Australia. Nature 375, 574–577.

Byerly, G.R., 1999. Komatiites of the Mendon Formation: late-stage ultramafic volcanism in the Barberton Greenstone Belt. Geol. Soc. Am. Spec. Paper 329, 189–211.

Condie, K.C., 1993. Chemical composition and evolution of the upper continental crust: contrasting results from surface samples and shales. Chem. Geol. 104, 1–37.

Condie, K.C., Wronkiewicz, D.J., 1990. The Cr/Th ratio in Precambrian pelites from the Kaapvaal Craton as an index of craton evolution. Earth Planet. Sci. Lett. 97, 256–267.

Corcoran, P.L., Mueller, W.U., Chown, E.H., 1998. Climatic and tectonic influences on fan deltas and wave- to tide-controlled shoreface deposits: evidence from the Archaean Keskarrah Formation, Slave Province, Canada. Sediment. Geol. 120, 125–152.

Corcoran, P.L., Mueller, W.U., Padgham, W.A., 1999. Influence of tectonism and climate on lithofacies distribution and sandstone and conglomerate composition in the Archean Beaulieu Rapids

Formation, Northwest Territories, Canada. Precambrian Res. 94, 175–204.

Cullers, R.L., Basu, A., Suttner, L.J., 1988. Geochemical signature of provenance in sand-size material in soils and stream sediments near the Tobacco Root batholith, Montana, USA. Chem. Geol. 70, 335–348.

Cullers, R.L., DiMarco, M.J., Lowe, D.R., Stone, J., 1993. Geochemistry of a silicified, felsic volcaniclastic suite from the early Archaean Panorama Formation, Pilbara Block. Western Australia: an evaluation of depositional and post-depositional processes with special emphasis on the rare-earth elements. Precambrian Res. 60, 99–116.

Cullers, R.L., Podkovyrov, V.N., 2002. The source and origin of terrigenous sedimentary rocks in the Mesoproterozoic Ui group, southeastern Russia. Precambrian Res. 117, 157–1183.

DiMarco, M.J., Lowe, D.R., 1989a. Petrography and provenance of silicified early Archaean volcaniclastic sandstones, eastern Pilbara Block, Western Australia. Sedimentology 36, 821–836.

DiMarco, M.J., Lowe, D.R., 1989b. Shallow-water volcaniclastic deposition in the Early Archean Panorama Formation, Warrawoona Group, eastern Pilbara Block, Western Australia. Sediment. Geol. 64, 43–63.

DiMarco, M.J., Lowe, D.R., 1989c. Stratigraphy and sedimentology of an early Archean felsic volcanic sequence, eastern Pilbara Block, Western Australia, with special reference to the Duffer Formation and implications for crustal evolution. Precambrian Res. 44, 147–169.

Donaldson, J.A., de Kemp, E.A., 1998. Archaean quartz arenites in the Canadian Shield: examples from the Superior and Churchill Provinces. Sediment. Geol. 120, 153–176.

Duchač, K.C., Hanor, J.S., 1987. Origin and timing of the metasomatic silicification of an early Archean komatiite sequence, Barberton Mountain Land, South Africa. Precambrian Res. 37, 125–146.

Fedo, C.M., Eriksson, K.A., Krogstad, E.J., 1996. Geochemistry of shales from the Archean (∼3.0 Ga) Buhwa Greenstone Belt, Zimbabwe: implications for provenance and source-area weathering. Geochim. Cosmochim. Acta 60, 1751–1763.

Fedo, C.M., Young, G.M., Nesbitt, H.W., 1997. Paleoclimatic control on the composition of the Paleoproterozoic Serpent Formation, Huronian Supergroup, Canada: a greenhouse to icehouse transition. Precambrian Res. 86, 201–223.

Feng, R., Kerrich, R., 1990. Geochemistry of fine-grained clastic sediments in the Archean Abitibi greenstone belt, Canada: implications for provenance and tectonic setting. Geochim. Cosmochim. Acta 54, 1061–1081.

Fralick, P.W., Kronberg, B.I., 1997. Geochemical discrimination of clastic sedimentary rock sources. Sediment. Geol. 113, 111–124.

Gao, S., Wedepohl, K.H., 1995. The negative Eu anomaly in Archean sedimentary rocks: implications for decomposition, age and importance of their granitic sources. Earth Planet Sci. Lett. 133, 81–94.

Garcia, D., Fonteilles, M., Moutte, J., 1994. Sedimentary fractionations between Al, Ti, and Zr and the genesis of strongly peraluminous granites. J. Geol. 102, 411–422.

Glikson, A.Y., Hickman, A.H., 1981. Geochemical stratigraphy and petrogenesis of Archaean basic-ultrabasic volcanic units, eastern Pilbara Block, Western Australia. Spec. Publs. Geol. Soc. Aust. 7, 287–300.

Green, M.G., Sylvester, P.J., Buick, R., 2000. Growth and recycling of early Archaean continental crust: geochemical evidence from the Coonterunah and Warrawoona Groups, Pilbara Craton, Australia. Tectonophysics 322, 69–88.

Hanor, J.S., Duchač, K.C., 1990. Isovolumetric silicification of early Archean komatiites: geochemical mass balances and constraints on origin. J. Geol. 98, 863–877.

Heaman, L.M., Bowins, R., Crocket, J., 1990. The chemical composition of igneous zircon suites: implications for geochemical tracer studies. Geochim. Cosmochim. Acta 54, 1597–1607.

Heinrichs, T.K., Reimer, T.O., 1977. A sedimentary barite deposit from the Archean Fig. Tree Group of the Barberton Mountain Land (South Africa). Econ. Geol. 72, 1426–1441.

Hickman, A.H., 1983. Geology of the Pilbara Block and its environs. West. Aust. Geol. Surv. Bull., 127.

Hofmann, A., 2005. The geochemistry of sedimentary rocks from the Fig Tree Group, Barberton greenstone belt: implications for tectonic, hydrothermal and surface processes during mid-Archaean times. Precambrian Res. 143, 23–49.

Hofmann, A., Bolhar, R., Dirks, P., Jelsma, H., 2003. The geochemistry of Archaean shales derived from a mafic volcanic sequence, Belingwe greenstone belt, Zimbabwe: provenance, source area unroofing and submarine versus subaerial weathering. Geochim. Cosmochim. Acta 67, 421–440.

Holland, H.D., 1984. The Chemical Evolution of the Atmosphere and Oceans. Princeton University Press, Princeton, NJ.

Jahn, B.-M., Glikson, A.Y., Peucat, J.J., Hickman, A.H., 1981. REE geochemistry and isotopic data of Archean silicic volcanics and granitoids from the Pilbara Block, Western Australia: implications for the early crustal evolution. Geochim. Cosmochim. Acta 45, 1633–1652.

Johnsson, M.J., 1993. The system controlling the composition of clastic sediments. In: Johnsson, M.J., Basu, A. (Eds.), Processes controlling the composition of clastic sediments. Geol., Soc. Am. Spec. Paper, 284, 1–19.

Kato, Y., Ikezaki, A., 2000. Geochemistry of early Archean (3.5 Gyr) siliceous mudstone and sandstone from the Marble Bar area in the Pilbara Craton, Western Australia. Mem. Geol. Soc. Jpn. 57, 171–181.

Lowe, D.R., 1980. Stromatolites 3400-Myr old from the Archean of Western Australia. Nature 284, 441–443.

Lowe, D.R., 1983. Restricted shallow-water sedimentation of Early Archean stromatolitic and evaporitic strata of the Strelley Pool Chert, Pilbara Block, Western Australia. Precambrian Res. 19, 239–283.

Lowe, D.R., 1999. Petrology and sedimentology of cherts and related silicified sedimentary rocks in the Swaziland Supergroup. Geol. Soc. Am. Spec. Paper 329, 83–114.

Lowe, D.R., Byerly, G.R., 1986. Archean flow-top alteration zones formed initially in a low-temperature sulphate-rich environment. Nature 324, 245–248.

Lowe, D.R., Knauth, L.P., 1977. Sedimentology of the Onverwacht Group (3.4 billion years), Transvaal, South Africa, and its bearing on the characteristics and evolution of the early earth. J. Geol. 85, 699–723.

Lowe, D.R., Tice, M.M., 2004. Geologic evidence for Archean atmospheric and climatic evolution: fluctuating levels of CO_2, CH_4, and O_2 with an overriding tectonic control. Geology 32, 493–496.

Lowe, D.R., Worrell, G.F., 1999. Sedimentology, mineralogy, and implications of silicified evaporites in the Kromberg Formation, Barberton Greenstone Belt, South Africa. Geol. Soc. Am. Bull. Spec. Paper 329, 167–188.

McLennan, S.M., Taylor, S.R., Eriksson, K.A., 1983. Geochemistry of Archean shales from the Pilbara Supergroup, Western Australia. Geochim. Cosmochim. Acta 47, 1211–1222.

McNaughton, N.J., Compston, W., Barley, M.E., 1993. Constraints on the age of the Warrawoona Group, eastern Pilbara Block, Western Australia. Precambrian Res. 60, 69–98.

Naqvi, S.M., Uday Raj, B., Subba Rao, D.V., Manikyamba, C., Nirmal Charan, S., Balaram, V., Srinivasa Sarma, D., 2002. Geology and geochemistry of arenite-quartzwacke from the Late Archaean Sandur schist belt—implications for provenance and accretion processes. Precambrian Res. 114, 177–197.

Nesbitt, H.W., Young, G.M., McLennan, S.M., Keays, R.R., 1996. Effects of chemical weathering and sorting on the petrogenesis of siliciclastic sediments, with implications for provenance studies. J. Geol. 104, 525–542.

Nesbitt, H.W., Fedo, C.M., Young, G.M., 1997. Quartz and feldspar stability, steady-state and non-steady weathering, and petrogenesis of siliciclastic sands and muds. J. Geol. 105, 173–191.

Nijman, W., de Bruijne, K.C.H., Valkering, M.E., 1998. Growth fault control of Early Archaean cherts, barite mounds and chert-barite veins, North Pole Dome, Eastern Pilbara, Western Australia. Precambrian Res. 88, 25–52.

Paris, I., Stanistreet, I.G., Hughes, M.J., 1985. Cherts of the Barberton greenstone belt interpreted as products of submarine exhalative activity. J. Geol. 93, 111–129.

Pirajno, F., Grey, K., 2002. Chert in the Palaeoproterozoic Bartle Member, Killara Formation, Yerrida Basin, Western Australia: a rift-related playa lake and thermal spring environment? Precambrian Res. 113, 169–192.

Pirajno, F., Van Kranendonk, M.J., 2005. Review of hydrothermal processes and systems on Earth and implications for Martian analogues. Aust. J. Earth Sci. 52, 329–351.

Polat, A., Hofmann, A.W., 2003. Alteration and geochemical patterns in the 3.7–3.8 Ga Isua greenstone belt, West Greenland. Precambrian Res. 126, 197–218.

Polat, A., Hofmann, A.W., Rosing, M.T., 2002. Boninite-like volcanic rocks in the 3.7–3.8 Ga Isua greenstone belt. West Greenland: geochemical evidence for intra-oceanic subduction zone processes in the early Earth. Chem. Geol. 184, 231–254.

Salvi, S., Williams-Jones, A.E., 1996. The role of hydrothermal processes in concentrating high-field strength elements in the Strange Lake peralkaline complex, northeastern Canada. Geochim. Cosmochim. Acta 60, 1917–1932.

Shibata, S., Tanaka, T., Minami, M., Senda, R., Takebe, M., Kachi, T., Kondo, M., Oda, S., Hayashi, T., Nishizawa, K., Kojima, H., 2001. The procedure and accuracy of INAA for geological materials by new γ-ray counting and data processing system at Radioisotope Center in Nagoya University. Bull. Nagoya Univ. Museum 17, 15–32.

Simonson, B.M., 1985. Sedimentology of cherts in the Early Proterozoic Wishart Formation, Quebec-Newfoundland, Canada. Sedimentology 32, 23–40.

Smithies, R.H., 2002. De Grey, W.A. Sheet 2757: Western Australia Geological Survey, 1:100 000 Geological Series.

Smithies, R.H., Hickman, A.H., Nelson, D.R., 1999. New constraints on the evolution of the Mallina Basin, and their bearing on relationships between the contrasting eastern and western granite-greenstone terranes of the Archaean Pilbara Craton, Western Australia. Precambrian Res. 94, 11–28.

Smithies, R.H., Van Kranendonk, M.J., Champion, D.C., 2005. It started with a plume—early Archaean basaltic proto-continental crust. Earth Planet. Sci. Lett. 238, 284–297.

Sugisaki, R., Shimomura, T., Ando, K., 1977. An automatic X-ray fluorescence method for the analysis of silicate rocks. J. Geol. Soc. Jpn. 83, 725–733.

Sugisaki, R., Yamamoto, K., Adachi, M., 1982. Triassic bedded cherts in central Japan are not pelagic. Nature 298, 644–647.

Sugitani, K., Horiuchi, Y., Adachi, M., Sugisaki, R., 1996. Anomalously low Al_2O_3/TiO_2 values for Archean cherts from the Pilbara Block. Western Australia—possible evidence for extensive chemical weathering on the early earth. Precambrian Res. 80, 49–76.

Sugitani, K., Mimura, K., 1998. Redox change in sedimentary environments of Triassic bedded cherts, central Japan: possible reflection of sea-level change. Geol. Mag. 135, 735–753.

Sugitani, K., Yamamoto, K., Wada, H., Binu-Lal, S.S., Yoneshige, M., 2002. Geochemistry of Archean carbonaceous cherts deposited at immature island-arc setting in the Pilbara Block, Western Australia. Sediment. Geol. 151, 45–66.

Sugitani, K., Mimura, K., Suzuki, K., Nagamine, K., Sugisaki, R., 2003. Stratigraphy and sedimentary petrology of an Archean volcanic-sedimentary succession at Mt. Goldsworthy in the Pilbara Block, Western Australia: implications of evaporite (nahcolite) and barite deposition. Precambrian Res. 120, 55–79.

Suzuki, K., Adachi, M., 1991. Precambrian provenance and Silurian metamorphism of Tsubonosawa paragneiss in the South Kitakami terrane, Northeast Japan, revealed by the chemical Th–U–total Pb isochron ages of monazite, zircon and xenotime. Geochem. J. 25, 357–376.

Suzuki, K., Adachi, M., Tanaka, T., 1991. Middle Precambrian provenance of Jurassic sandstone in the Mino Terrane, central Japan: Th–U–total Pb evidence from an electron microprobe monazite study. Sediment. Geol. 75, 141–147.

Taylor, S.R., McLennan, S.M., 1985. The Continental Crust: Its Composition and Evolution. Blackwell Scientific Publications, Oxford.

Thorpe, R.I., Hickman, A.H., Davis, D.W., Mortensen, J.K., Trendall, A.F., 1992. U–Pb zircon geochronology of Archaean felsic units in the Marble Bar region, Pilbara Craton, Western Australia. Precambrian Res. 56, 169–189.

Van Kranendonk, M.J., Hickman, A.H., Smithies, R.H., Nelson, D.R., 2002. Geology and tectonic evolution of the Archean North Pilbara Terrane, Pilbara Craton, Western Australia. Econ. Geol. 97, 695–732.

Van Kranendonk, M.J., Smithies, R.H., Hickman, A.H., Bagas, L., Williams, I.R., Farrell, T.R., 2003-04. Event stratigraphy applied to 700 million years of Archaean crustal evolution, Pilbara Craton, Western Australia. Geol. Soc. West. Aust. Ann. Rev., 49–61.

Van Kranendonk, M.J., Pirajno, F., 2004. Geochemistry of metabasalts and hydrothermal alteration zones associated with *c.* 3.45 Ga chert and barite deposits: implications for the geological setting of the Warrawoona Group, Pilbara Craton, Australia. Explor. Environ. Anal. 4, 253–278.

Van Kranendonk, M.J., 2006. Volcanic degassing, hydrothermal circulation and the flourishing of early life on Earth: a review of the evidence from c. 3490–3240 Ma rocks of the Pilbara Supergroup, Pilbara Craton, Western Australia. Earth-Sci. Rev. 74, 197–240.

Whitehouse, M.J., Kamber, B.S., 2003. A rare earth element study of complex zircons from early Archaean Amîtsoq gneisses, Godthåbsfjord, south-west Greenland. Precambrian Res. 126, 363–377.

Wronkiewicz, D.J., Condie, K.C., 1987. Geochemistry of Archean shales from the Witwatersrand Supergroup, South Africa: source-area weathering and provenance. Geochim. Cosmochim. Acta 51, 2401–2416.

Wronkiewicz, D.J., Condie, K.C., 1989. Geochemistry and provenance of sediments from the Pongola Supergroup, South Africa: evidence for a 3.0-Ga-old continental craton. Geochim. Cosmochim. Acta 53, 1537–1549.

Young, G.M., Nesbitt, H.W., 1998. Processes controlling the distribution of Ti and Al in weathering profiles, siliciclastic sediments and sedimentary rocks. J. Sediment. Res. 68, 448–455.